TREM2 mutations implicated in neurodegeneration impair cell surface transport and phagocytosis

ARTICLE *in* SCIENCE TRANSLATIONAL MEDICINE · JULY 2014

Impact Factor: 15.84 · DOI: 10.1126/scitranslmed.3009093

33 AUTHORS, INCLUDING:

Gernot Kleinberger
Ludwig-Maximilians-University of Munich
24 PUBLICATIONS **819** CITATIONS
SEE PROFILE

Marc Suárez-Calvet
Ludwig-Maximilians-University of Munich
25 PUBLICATIONS **901** CITATIONS
SEE PROFILE

Juan Fortea
Hospital de la Santa Creu i Sant Pau
67 PUBLICATIONS **467** CITATIONS
SEE PROFILE

Sebastiaan Engelborghs
University of Antwerp
339 PUBLICATIONS **9,873** CITATIONS
SEE PROFILE

NEURODEGENERATIVE DISEASE

TREM2 mutations implicated in neurodegeneration impair cell surface transport and phagocytosis

Gernot Kleinberger,[1,2] Yoshinori Yamanishi,[3] Marc Suárez-Calvet,[1,4,5] Eva Czirr,[6,7] Ebba Lohmann,[8,9,10] Elise Cuyvers,[11,12] Hanne Struyfs,[13] Nadine Pettkus,[1] Andrea Wenninger-Weinzierl,[14] Fargol Mazaheri,[14] Sabina Tahirovic,[14] Alberto Lleó,[4,5] Daniel Alcolea,[4,5] Juan Fortea,[4,5] Michael Willem,[1] Sven Lammich,[1] José L. Molinuevo,[15] Raquel Sánchez-Valle,[15] Anna Antonell,[15] Alfredo Ramirez,[16,17] Michael T. Heneka,[18,19] Kristel Sleegers,[11,12] Julie van der Zee,[11,12] Jean-Jacques Martin,[20] Sebastiaan Engelborghs,[13,21] Asli Demirtas-Tatlidede,[8] Henrik Zetterberg,[22,23] Christine Van Broeckhoven,[11,12] Hakan Gurvit,[8] Tony Wyss-Coray,[6,7,24] John Hardy,[23] Marco Colonna,[3] Christian Haass[1,2,14]*

Genetic variants in the triggering receptor expressed on myeloid cells 2 (TREM2) have been linked to Nasu-Hakola disease, Alzheimer's disease (AD), Parkinson's disease, amyotrophic lateral sclerosis, frontotemporal dementia (FTD), and FTD-like syndrome without bone involvement. TREM2 is an innate immune receptor preferentially expressed by microglia and is involved in inflammation and phagocytosis. Whether and how TREM2 missense mutations affect TREM2 function is unclear. We report that missense mutations associated with FTD and FTD-like syndrome reduce TREM2 maturation, abolish shedding by ADAM proteases, and impair the phagocytic activity of TREM2-expressing cells. As a consequence of reduced shedding, TREM2 is virtually absent in the cerebrospinal fluid (CSF) and plasma of a patient with FTD-like syndrome. A decrease in soluble TREM2 was also observed in the CSF of patients with AD and FTD, further suggesting that reduced TREM2 function may contribute to increased risk for two neurodegenerative disorders.

INTRODUCTION

Homozygous loss-of-function mutations in the triggering receptor expressed on myeloid cells 2 (*TREM2*) gene cause polycystic lipomembranous osteodysplasia with sclerosing leukoencephalopathy [also known as Nasu-Hakola disease (NHD)], a disease characterized by ankle swellings and frequent bone fractures (*1*). During disease progression, NHD patients develop neurological syndromes reminiscent of the behavioral variant of frontotemporal dementia (FTD) (*1*). Recently, homozygous missense mutations of TREM2, such as the p.T66M and the p.Y38C mutations, as well as a compound heterozygous missense mutation have been identified to cause an FTD-like syndrome without bone pathology (*2*, *3*). Genetic screenings have now also identified heterozygous missense mutations in TREM2 as risk factors for Alzheimer's disease (AD), Parkinson's disease (PD), amyotrophic lateral sclerosis (ALS), and FTD (*4*–*9*). Most reported missense mutations are located in the ectodomain of TREM2, a membrane-bound type 1 protein (Fig. 1A). Integrated network analysis suggested a central role for TREM2 in various brain areas (*10*), where it is mainly expressed in microglia cells regulating essential functions including phagocytosis and the removal of apoptotic neurons (*11*–*14*).

The TREM2 homolog TREM1 is found as a soluble variant in the serum of patients with septic shock and is secreted from monocytes upon stimulation with lipopolysaccharide (*15*). Furthermore, TREM2 was also observed in plasma and cerebrospinal fluid (CSF) samples from patients with multiple sclerosis (*16*). In line with these findings, recent evidence suggests that TREM2 is a substrate for regulated intramembrane proteolysis (RIP) (*17*). RIP substrates are membrane-bound proteins, whose ectodomains are released upon shedding by proteases such as members of the ADAM (a disintegrin and metalloproteinase domain-containing protein) or BACE (β-site APP cleaving enzyme) family (*18*). Upon removal of the ectodomain, the remaining membrane-retained stub is further processed by intramembrane proteolysis (*19*).

Whether and how missense mutations affect TREM2 function is elusive. Here, we investigated whether TREM2 missense mutations found in patients with FTD, FTD-like syndrome without bone involvement, AD, and other neurodegenerative diseases affect the transport and processing of the TREM2 protein and thus may cause its loss of function.

[1]Adolf-Butenandt Institute, Biochemistry, Ludwig-Maximilians University Munich, 80336 Munich, Germany. [2]Munich Cluster for Systems Neurology (SyNergy), 80336 Munich, Germany. [3]Department of Pathology and Immunology, Washington University School of Medicine, St. Louis, MO 63110, USA. [4]Department of Neurology, Institut d'Investigacions Biomèdiques, Hospital de la Santa Creu i Sant Pau, Universitat Autònoma de Barcelona, 08025 Barcelona, Spain. [5]Center for Networked Biomedical Research for Neurodegenerative Diseases, CIBERNED, 28031 Madrid, Spain. [6]Department of Neurology and Neurological Sciences, Stanford University School of Medicine, Stanford, CA 94305, USA. [7]Center for Tissue Regeneration, Repair and Restoration, Veterans Administration Palo Alto Health Care System, Palo Alto, CA 94304, USA. [8]Behavioral Neurology and Movement Disorders Unit, Department of Neurology, Istanbul Faculty of Medicine, Istanbul University, 34093 Istanbul, Turkey. [9]Department of Neurodegenerative Diseases, Hertie Institute for Clinical Brain Research, University of Tübingen, 72076 Tübingen, Germany. [10]German Center for Neurodegenerative Diseases (DZNE), Tübingen, 72076 Tübingen, Germany. [11]Neurodegenerative Brain Diseases Group, Department of Molecular Genetics, VIB, 2610 Antwerp, Belgium. [12]Laboratory of Neurogenetics, Institute Born-Bunge, University of Antwerp, 2610 Antwerp, Belgium. [13]Reference Center for Biological Markers of Dementia, Laboratory of Neurochemistry and Behavior, Institute Born-Bunge, University of Antwerp, 2610 Antwerp, Belgium. [14]German Center for Neurodegenerative Diseases (DZNE), Munich, 80336 Munich, Germany. [15]Alzheimer's Disease and Other Cognitive Disorders Unit, Neurology Service, ICN Hospital Clinic i Universitari, 08036 Barcelona, Spain. [16]Department of Psychiatry and Psychotherapy, University of Bonn, 53127 Bonn, Germany. [17]Institute of Human Genetics, University of Bonn, 53127 Bonn, Germany. [18]Universitätsklinikum Bonn, Neurology, 53127 Bonn, Germany. [19]German Center for Neurodegenerative Diseases (DZNE), 53127 Bonn, Germany. [20]Antwerp Biobank, Institute Born-Bunge, University of Antwerp, 2610 Antwerp, Belgium. [21]Department of Neurology and Memory Clinic, Hospital Network Antwerp (ZNA), Middelheim and Hoge Beuken, 2020 Antwerp, Belgium. [22]Institute of Neuroscience and Physiology, Department of Psychiatry and Neurochemistry, The Sahlgrenska Academy at the University of Gothenburg, S-431 80 Mölndal, Sweden. [23]Reta Lila Weston Laboratories and Department of Molecular Neuroscience, UCL Institute of Neurology, London WC1N 3BG, UK. [24]Neuroscience IDP Program, Stanford University School of Medicine, Stanford, CA 94305, USA.
*Corresponding author. E-mail: christian.haass@dzne.lmu.de

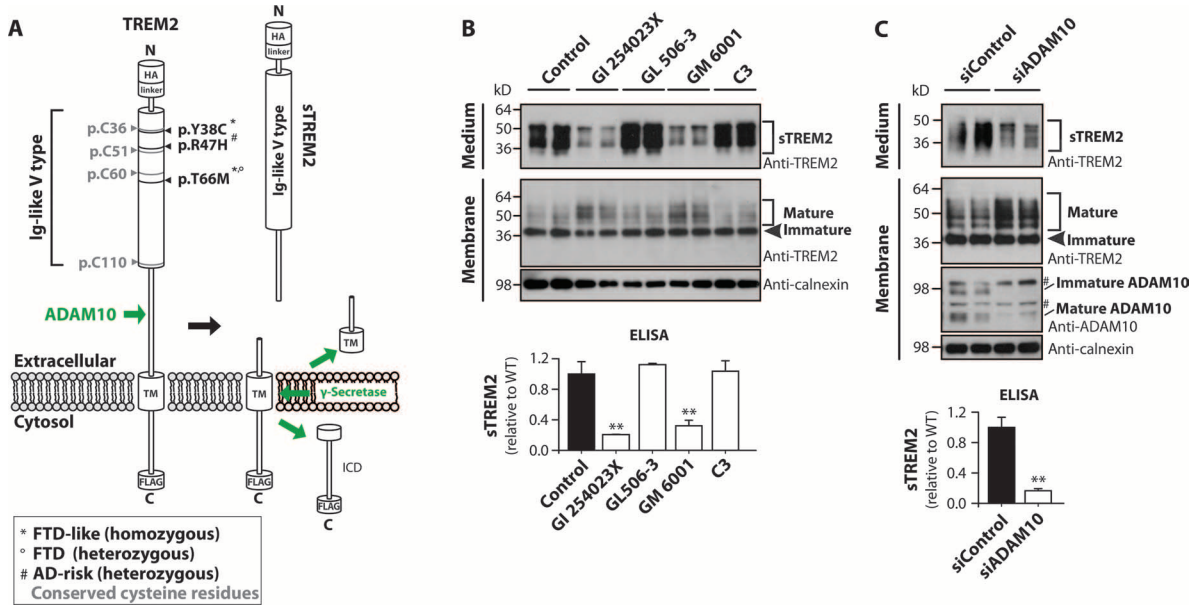

Fig. 1. TREM2 is shed by ADAM10 in HEK293 Flp-In cells. (**A**) Illustration of membrane-bound TREM2. Upon shedding by ADAM10, the remaining C-terminal stub of TREM2 is cleaved within the membrane by γ-secretase (*17*). Ig, immunoglobulin; HA, hemagglutinin; TM, transmembrane domain; ICD, intracellular domain. (**B**) Pharmacological inhibition of ADAM proteases using a broad ADAM inhibitor (GM 6001) or a more selective ADAM10 inhibitor (GI 254023X) but not a more selective ADAM17 (GL 506-3) or BACE1 (C1) inhibitor reduced sTREM2 generation and stabilized fully glycosylated, cell surface–associated, mature membrane-bound wild-type (WT) TREM2. (**C**) Small interfering RNA (siRNA)–mediated ADAM10 knockdown confirmed reduced ADAM10-mediated TREM2 shedding. Hashtags indicate nonspecific immunoreactivity. Anti-calnexin antibody (B and C) was used as a loading control. Bar graphs (B and C) show enzyme-linked immunosorbent assay (ELISA) quantification of sTREM2 relative to control-treated cells. Quantitative data are represented as means ± SD from at least two independent experiments; $n = 4$ to 7 (B) and $n = 8$ (C). Statistical differences were calculated by Mann-Whitney U test. $^{**}P < 0.01$.

RESULTS

Generation of soluble TREM2 by ADAM10-mediated ectodomain shedding

Soluble fragments of TREM2 (sTREM2) have been observed in supernatants of dendritic cell cultures as well as in plasma and CSF samples from patients with noninflammatory neurological diseases and multiple sclerosis (*16*). Consistent with that, we observed secreted fragments of TREM2 (Fig. 1B) migrating as multiple bands in the range of 36 to 50 kD as well as the full-length membrane-bound TREM2 migrating between 36 and 60 kD (Fig. 1B) in isogenic human embryonic kidney 293 cells (HEK293 Flp-In) stably expressing a single copy of human wild-type TREM2. We did not find C-terminal FLAG epitope containing fragments in the conditioned medium, implying that sTREM2 is produced by ectodomain shedding (fig. S1). Moreover, in HEK293 Flp-In cells, the broad ADAM inhibitor GM 6001 reduced secretion of sTREM2 as did the more selective ADAM10 inhibitor GI 254023X, but not the ADAM17-specific inhibitor GL 506-3 or the BACE inhibitor C3 (Fig. 1B). Reduced sTREM2 correlated with an increase in fully glycosylated mature membrane-bound TREM2 (Fig. 1B, middle panel; for further analysis of immature and mature TREM2, see the pulse-chase experiment in Fig. 2E and the deglycosylation experiments in fig. S2). siRNA-mediated knockdown revealed ADAM10 as a major sheddase of TREM2 in HEK293 Flp-In cells (Fig. 1C).

Impaired cell surface transport of mutant TREM2

Expression of the FTD and FTD-like TREM2 p.T66M and p.Y38C mutations (*2*, *9*) revealed a strong reduction of sTREM2 in conditioned medium from isogenic HEK293 Flp-In cells (Fig. 2A). Furthermore, the TREM2 p.R47H mutation, which increases the risk for AD, PD, and ALS (*4*–*7*), also showed reduced secretion of sTREM2 albeit to a lower extent (Fig. 2A). In parallel, we observed an accumulation of membrane-bound immature full-length TREM2 p.T66M and p.Y38C together with a reduction in TREM2 C-terminal fragments (CTFs) generated by ADAM10-mediated proteolytic cleavage (Fig. 2B). The detection of accumulating amounts of immature mutant TREM2 variants also confirmed that the mutations do not abolish antibody recognition. Consistent with a weaker effect of the p.R47H mutation on TREM2 shedding, we observed a much less marked accumulation of immature p.R47H mutant TREM2 (Fig. 2B; quantitated in Fig. 2C). Mutagenesis of conserved cysteine residues (p.C36A and p.C60A) blocked TREM2 shedding like the p.T66M and p.Y38C mutations (Fig. 2A) and caused an accumulation of immature membrane-bound full-length TREM2 as well as a reduction of the CTF (Fig. 2B). This further supports the possibility that mutant TREM2 is misfolded and retained within the cell. Coexpression of DAP12, the signaling adaptor for TREM2 (*20*), which is not expressed in HEK293 Flp-In cells, did not restore transport and shedding of mutant TREM2 (Fig. 2D). Pulse-chase experiments showed that wild-type membrane-bound full-length TREM2 matured from a low–molecular weight immature species to a higher–molecular weight mature species most likely by glycosylation (Fig. 2E and fig. S2). Upon maturation after 60 to 90 min of cold chase, TREM2 was shed and accumulated over time in the conditioned medium (Fig. 2E). In contrast to wild-type TREM2, mutant p.T66M TREM2 failed to mature efficiently, resulting in the accumulation of immature TREM2 in the cell

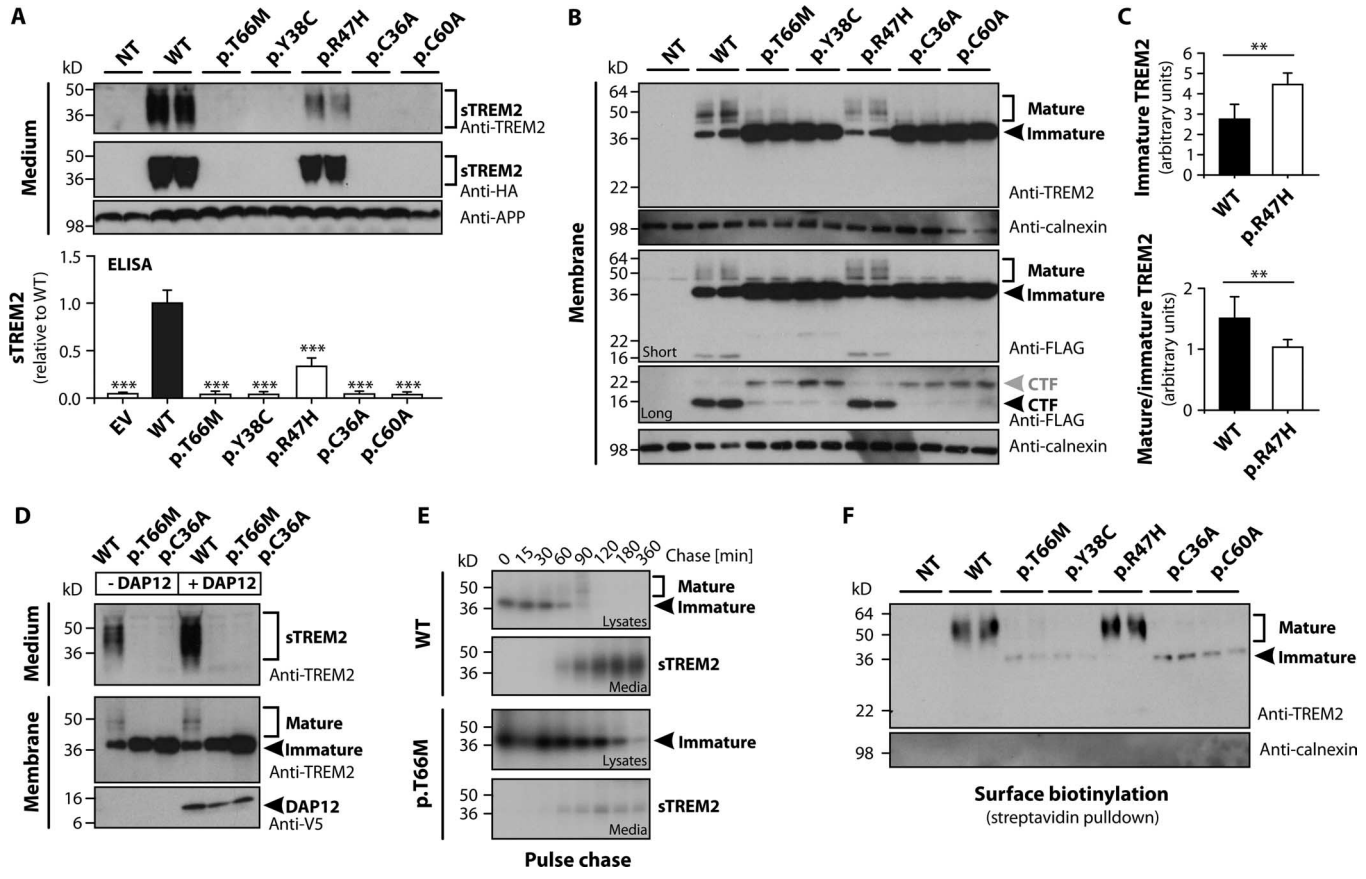

Fig. 2. Reduced cell surface transport and shedding of mutant TREM2. (**A**) Anti-TREM2 and anti-HA immunoblotting of sTREM2 in supernatants from cells expressing the FTD- and FTD-like–associated TREM2 mutations p.T66M and p.Y38C or mutations of conserved cysteine residues at positions 36 and 60. Lower panel shows quantification of sTREM2 by ELISA on supernatants from stable HEK293 Flp-In cells. (**B**) Immature mutant TREM2 (black arrowhead) accumulated, whereas the mature form and CTFs were reduced compared to WT TREM2. An alternative proteolytic event appears to produce minor amounts of a larger CTF (gray arrowhead). (**C**) Quantification of immunoblots shows a small increase in immature p.R47H TREM2 and a significant decrease in the ratio of mature-to-immature TREM2. (**D**) Coexpression of DAP12, the signaling adaptor of TREM2, did not affect reduced maturation and secretion of mutant TREM2. (**E**) Pulse-chase experiments revealed a longer half-life for mutant TREM2 within cell lysates accompanied by a minimal release of sTREM2 into the medium. (**F**) Surface biotinylation of mature surface-exposed mutant TREM2. Anti-APP (A) or anti-calnexin (B) antibodies were used as loading controls for supernatants or membrane fractions, respectively. Anti-calnexin antibody was used to prove selective cell surface labeling. NT, non-transfected HEK293 Flp-In host cell line. Quantitative data are represented as means ± SD from three independent experiments using three independent cell lines for WT or p.R47H TREM2. $n > 6$ (A) and $n = 9$ (C). Statistical differences were calculated by Mann-Whitney U test. $^{**}P < 0.01$; $^{***}P < 0.001$.

lysate and inefficient generation of sTREM2 (Fig. 2E). Accordingly, cell surface TREM2 was decreased upon expression of the TREM2 p.T66M, p.Y38C, p.C36A, and p.C60A mutants compared to wild-type TREM2 (Fig. 2F). Consistent with less marked effects of the p.R47H mutation on TREM2 maturation and sTREM2 generation, p.R47H TREM2 showed similar cell surface expression compared to wild-type TREM2 (Fig. 2F). Immunohistochemistry also showed severely reduced cell surface expression of TREM2 p.T66M, p.Y38C, p.C36A, and p.C60A accompanied by an increase of intracellular staining, which colocalized preferentially with the endoplasmic reticulum (ER) marker calnexin (Fig. 3A). Consistent with our biochemical findings, the p.R47H TREM2 mutation showed less intracellular accumulation (Fig. 3A), and consequently, robust expression of cell surface TREM2 was detected (Fig. 3B). Thus, mutations associated with FTD and FTD-like syndrome affected TREM2 maturation, cell surface transport, and proteolytic processing, whereas the AD-associated p.R47H mutation had a mild effect on maturation and secretion, which is at the limit of biochemical detection.

Reduced maturation and shedding of mutant TREM2 in microglial cells

Within the human brain, TREM2 is primarily expressed in microglia cells (*11*–*14*). Therefore, we aimed to confirm our findings in an in vivo relevant setting. To do so, we expressed wild-type TREM2, as well as the TREM2 mutations p.T66M, p.Y38C, p.R47H, and p.C36A, in the murine microglial BV2 cell line, a model frequently used for in vitro studies of microglial function (*21*–*23*). Reverse transcription polymerase chain reaction (RT-PCR) analysis confirmed the expression of selected microglial markers *CD11b* and *CD68* as well as the expression of *Trem2* and *Dap12* in the BV2 cell line (Fig. 4A). The p.T66M, p.Y38C, and p.C36A mutations exhibited reduced shedding of sTREM2 in BV2 cells (Fig. 4B), as observed in HEK293 Flp-In cells (Fig. 2A). Remarkably, the TREM2 p.R47H mutant consistently showed reduced expression in the membrane fraction of transiently transfected BV2 cells (Fig. 4B), an observation that was also confirmed in stably transfected BV2 cell lines (fig. S3). Nevertheless, similar to our findings in HEK293 Flp-In cells

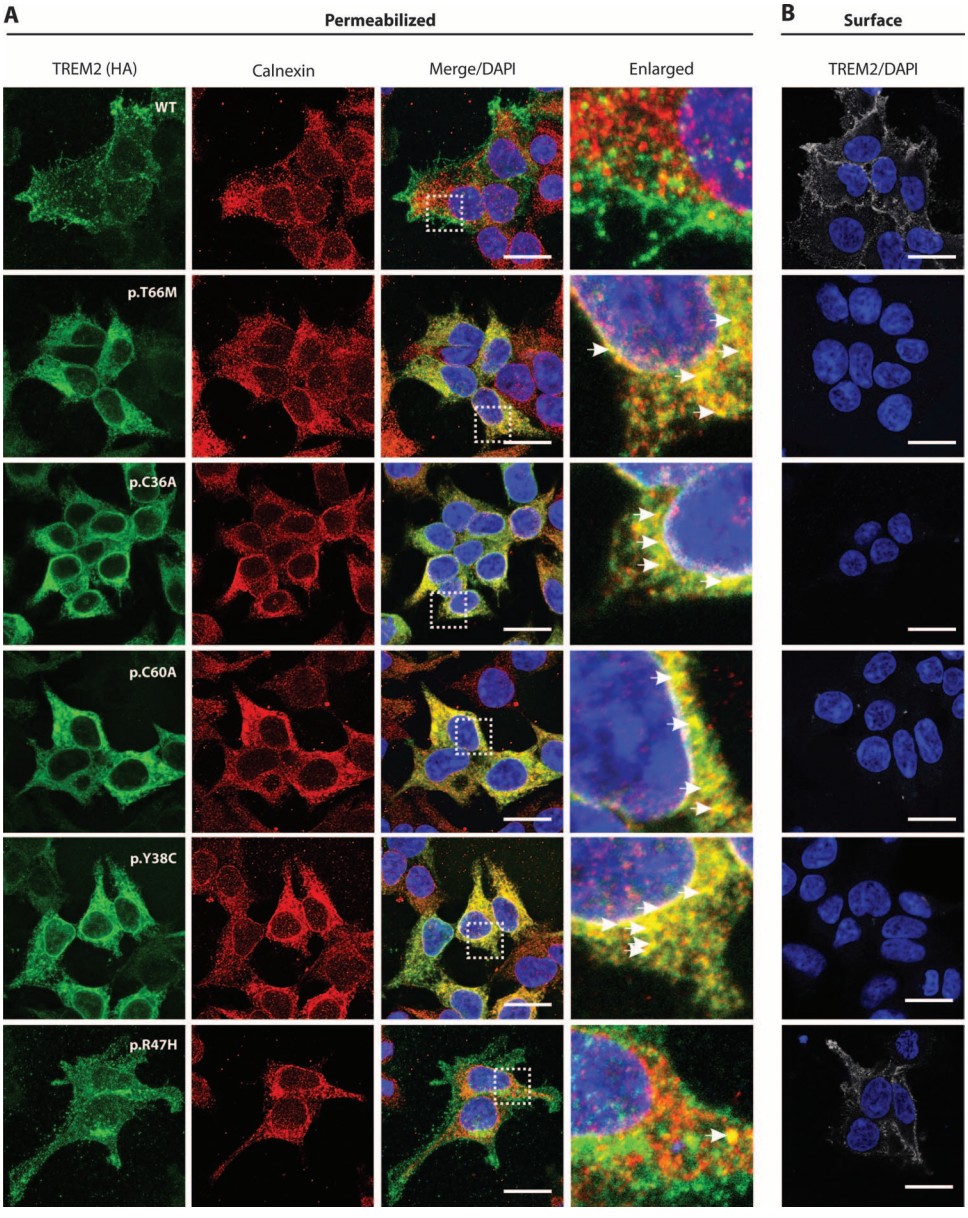

Fig. 3. Mutant TREM2 accumulates in the cytoplasm of stable HEK293 Flp-In cells. (**A**) Double immunofluorescence of TREM2 labeled with anti-HA antibody and anti-calnexin antibody. White boxes on the merged images depict the enlarged area shown in the images to the right. White arrows in enlarged images highlight selected areas showing TREM2 and calnexin colocalization. (**B**) Surface staining of WT and mutant TREM2-expressing HEK293 Flp-In cells. Scale bars, 10 μm. DAPI, 4′,6-diamidino-2-phenylindole.

(Fig. 2A), the p.R47H mutation showed reduced secretion of sTREM2 (Fig. 4B). Shedding of TREM2 by microglia cells was also mediated by proteases of the ADAM family but not BACE1 (Fig. 4C). In the microglia BV2 cell line, both ADAM10 and ADAM17 contributed to shedding of TREM2 (Fig. 4C). We also confirmed reduced cell surface transport of mutant TREM2 in BV2 cells by investigating wild-type and p.T66M mutant TREM2 in a cell surface biotinylation assay. In line with our findings in HEK293 Flp-In cells, we found less cell surface TREM2 upon expression of the p.T66M mutation (Fig. 4D). Moreover, immunohistochemistry also fully confirmed the retention of mutant TREM2 in BV2 cells (Fig. 4E). Although wild-type TREM2 was predominantly observed in the Golgi, the p.T66M, p.Y38C, and p.C36A mutant variants were retained predominantly within the ER (Fig. 4E). Consistent with reduced effects of the p.R47H mutation on maturation of TREM2 and sTREM2 generation, this variant was predominantly located within the Golgi (Fig. 4E). Thus, the effects of TREM2 mutations on reduced maturation and cell surface transport as well as on proteolytic processing were confirmed in the microglial BV2 cell line.

Reduced sTREM2 in the CSF of patients with AD and FTD

To obtain evidence for reduced cell surface transport of mutant TREM2 in patients with FTD-like syndrome without bone involvement, we analyzed sTREM2 concentrations in the CSF and plasma of a patient carrying the TREM2 p.T66M mutation (*2*) as well as another patient with the p.Q33X mutation (*2*) for which only plasma was available. We established a highly sensitive sTREM2 ELISA (fig. S4, A to D) that showed good correlation with a previously published sTREM2 ELISA (*16*), which used independent antibodies (fig. S4B; Spearman rho = +0.521, $P < 0.001$). Consistent with the tissue culture analysis, these two independent ELISAs as well as immunoblotting revealed the virtual absence of sTREM2 in CSF from a patient with a homozygous TREM2 p.T66M mutation (Fig. 5A and fig. S4, E and F). Furthermore, the plasma concentration of sTREM2 in this patient was also below the detection limit and that of the patient carrying the p.Q33X mutation was very low (Fig. 5B). Because TREM2 is genetically linked not only to NHD and FTD-like syndrome without bone involvement but also to AD (*4*, *5*) and FTD (*6*, *8*, *9*), we analyzed sTREM2 concentrations in CSF samples of a set of well-characterized FTD and AD patients (Table 1) and compared them with those of neurologically normal controls. Although we observed an overlap between both groups, statistical analysis revealed a significant reduction of sTREM2 in AD and FTD patients compared to control individuals (Table 1 and Fig. 5A; $P = 0.001$ and $P < 0.001$, respectively, Mann-Whitney *U* test). The significant decrease in sTREM2 concentrations in CSF in AD and FTD patients compared to controls was still present after controlling for the effect of gender and age, and was independent of the clinics collecting CSF [$P = 0.001$ and $P < 0.001$, respectively, analysis of covariance (ANCOVA)]. In contrast to CSF measurements, we did not detect any

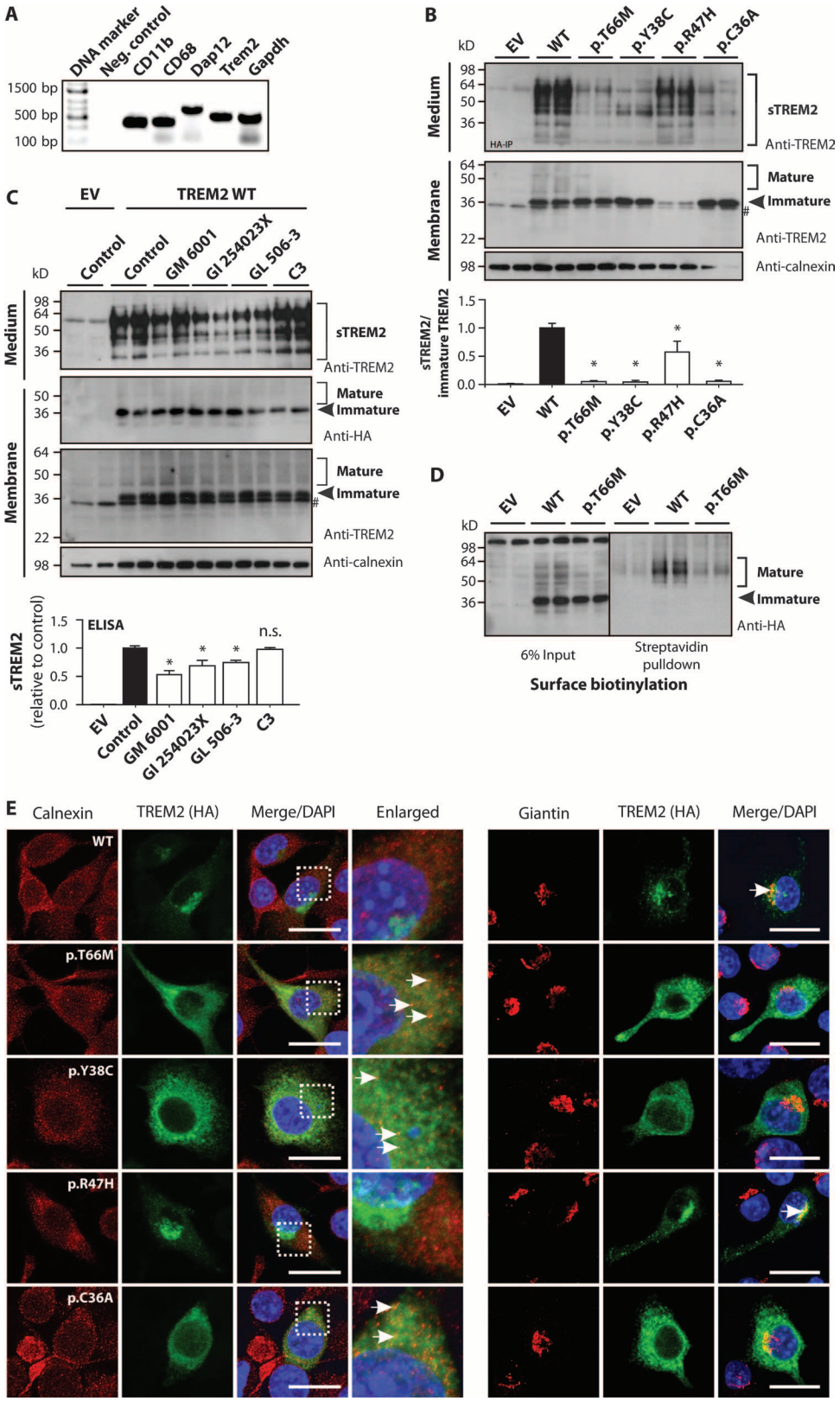

Fig. 4. Altered localization and reduced shedding of mutant TREM2 in BV2 microglial cells. (**A**) RT-PCR analysis of *Trem2*, *Dap12*, and microglial markers (*CD11b* and *CD68*) in BV2 cells. (**B**) Comparison of TREM2 processing in BV2 cells transiently expressing WT or mutant TREM2. Note that expression of the p.R47H variant was lower in all conducted experiments. Quantification of sTREM2 by ELISA normalized to the expression of immature TREM2 (lower panel). The AD variant p.R47H also showed reduced sTREM2 generation, but to a lesser extent than the other studied mutants. Hashtag indicates a protein that cross-reacts with the human anti-TREM2 antibody. (**C**) Similar to the case with HEK293 Flp-In cells (see Fig. 1), pharmacologic inhibition of ADAM proteases with GM 6001 (broad ADAM inhibitor), GI 254023X (ADAM10 inhibitor), and GL 506-3 (ADAM17 inhibitor) reduced the generation of sTREM2 in the microglial BV2 cell line. Anti-calnexin antibody was used as a loading control for membrane fractions in (B) and (C). (**D**) Surface biotinylation of mature surface-exposed mutant TREM2. (**E**) Double immunofluorescence of TREM2 labeled with anti-HA antibody and anti-calnexin antibody. White boxes on the merged images depict the area enlarged in the images to the right. White arrows in enlarged images highlight selected areas with TREM2 and calnexin colocalization. Scale bars, 20 μm. Quantitative data are represented as means ± SD from at least two independent experiments; $n = 4$. Statistical differences were calculated by Mann-Whitney *U* test. $^*P < 0.05$; n.s., nonsignificant.

difference in sTREM2 concentrations in plasma among the controls and the AD and FTD patients (Table 2 and Fig. 5B; $P = 0.872$, Kruskal-Wallis).

Impaired phagocytosis in TREM2 mutant cells

Reduction of cell surface TREM2 in microglia cells, the cell type in which TREM2 is selectively expressed within the brain, was reported to reduce removal of cellular debris and apoptotic neurons (*14*). In line with this, primary microglia from Trem2 knockout mice ($Trem2^{-/-}$) (*24*), which do not produce detectable sTrem2 in conditioned medium (Fig. 6A), showed a reduced phagocytic capacity compared to wild-type controls in an assay using *Escherichia coli* conjugated to pHrodo that only

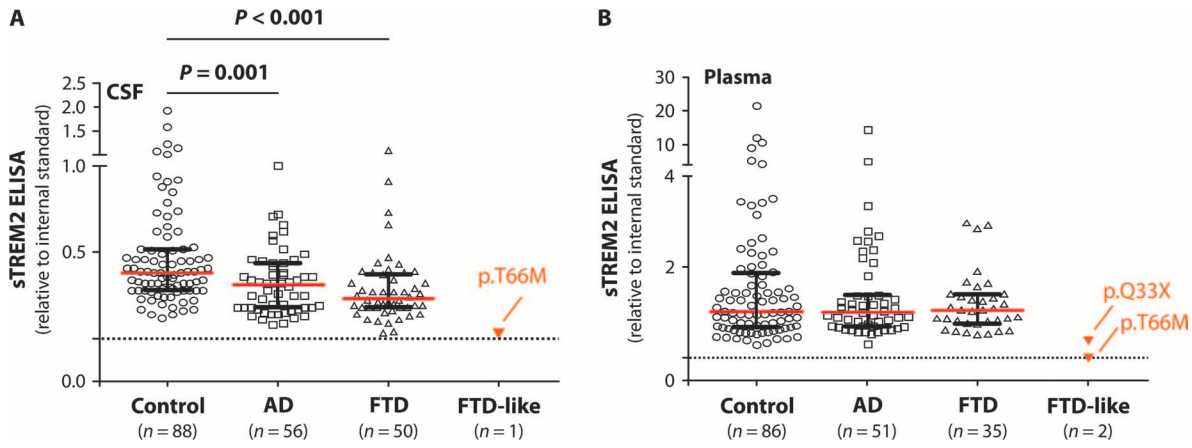

Fig. 5. Reduced sTREM2 in the CSF of patients with FTD and FTD-like syndrome. (**A**) ELISA-based analysis of sTREM2 in CSF samples shows virtual absence of sTREM2 in the TREM2 p.T66M mutation carrier, whereas robust concentrations of sTREM2 were detected in all control samples (n = 88). A reduction in sTREM2 was observed in AD patients (n = 56; $P_{\text{control vs. AD}}$ = 0.001) and FTD patients (n = 50; $P_{\text{control vs. FTD}}$ < 0.001). Horizontal bars indicate median sTREM2 concentrations per group with the interquartile range (IQR). (**B**) sTREM2 concentrations in plasma (n_{Control} = 86; n_{AD} = 51; n_{FTD} = 35) showed no significant difference among these groups. Plasma from the homozygous TREM2 p.T66M mutation carrier was the only sample (1 of 174 samples) with undetectable sTREM2. Additionally, plasma from a homozygous TREM2 p.Q33X mutation carrier (*2*) also showed one of the lowest sTREM2 concentrations of all measured samples.

Table 1. Characteristics of patient and control study population used to measure CSF sTREM2. Data are expressed as number of patients (percent), mean ± SD, or median (IQR) as appropriate. Probability values (P) denote differences between control, AD, and FTD patient groups. χ^2 tests were used for gender. One-way analysis of variance (ANOVA) was used to compare age between groups followed by Tukey post hoc test. CSF biomarkers and sTREM2 were evaluated by nonparametric statistical analysis (Kruskal-Wallis and post hoc with Mann-Whitney U test).

Variable	Total (n = 194)	Control (n = 88)	AD (n = 56)	FTD (n = 50)	P
Gender (F/M), no. (%)	113 (58)/81 (42)	55 (63)/33 (37)	38 (68)/18 (32)	20 (40)/30 (60)	0.008*
Age, years (mean ± SD)	64.6 ± 10.1	60.7 ± 9.5	70.4 ± 8.9	65.0 ± 9.4	<0.001†
CSF biomarkers					
$A\beta_{1-42}$ (pg/ml), median (IQR)	640.5 (460–824)	779.3 (643–914)	416.5 (312–526)	640.3 (491–829)	<0.001‡
T-tau (pg/ml), median (IQR)	254.7 (175–498)	204.3 (153–242)	665.3 (492–910)	256.1 (203–356)	<0.001§
P-tau_{181P} (pg/ml), median (IQR)	46.5 (37–69)	39.5 (35–50)	88.3 (67–103)	40.8 (30–51)	<0.001¶
sTREM2 (relative units)					
Median (IQR)	0.323 (0.201–0.448)	0.381 (0.283–0.518)	0.309 (0.178–0.436)	0.231 (0.180–0.370)	<0.001‖

*Post hoc significances for gender: controls versus AD, P = 0.512; controls versus FTD, P = 0.011; AD versus FTD, P = 0.004. †Post hoc significances for age: controls versus AD, P < 0.001; controls versus FTD, P = 0.025; AD versus FTD, P = 0.009. ‡Post hoc significances for $A\beta_{1-42}$: controls versus AD, P < 0.001; controls versus FTD, P = 0.001; AD versus FTD, P < 0.001. §Post hoc significances for T-tau: controls versus AD, P < 0.001; controls versus FTD, P < 0.001; AD versus FTD, P < 0.001. ¶Post hoc significances for P-tau_{181P}: controls versus AD, P < 0.001; controls versus FTD, P = 0.865; AD versus FTD, P < 0.001. ‖Post hoc significances for sTREM2: controls versus AD, P = 0.001; controls versus FTD, P < 0.001; AD versus FTD, P = 0.271.

yields a fluorescent signal in an acidic compartment (Fig. 6, B and C). Although the overall capacity of $Trem2^{-/-}$ microglia to phagocytose *E. coli* was only slightly reduced, $Trem2^{-/-}$ microglia seemed to be less competent in phagocytosing a larger amount of bacteria (Fig. 6, B and C).

Because our analysis in both the BV2 microglial cell line and the HEK293 Flp-In cells (Figs. 2 to 4) revealed reduced transport of mutant TREM2 to the cell surface, we next investigated whether this would correlate with a reduced capacity for phagocytosis. Consistent with that, bead uptake assays using HEK293 Flp-In cells expressing the ectodomain of TREM2 fused to the transmembrane and signaling domain of DAP12 (*25*, *26*) (Fig. 6, D and E) demonstrated that reduced cell surface localization and secretion of mutant TREM2 (p.T66M and p.Y38C) directly correlated with a reduced phagocytic capacity using opsonized fluorescent latex beads (Fig. 6F; **P = 0.004, Mann-Whitney U test). Moreover, an independent assay using *E. coli* conjugated to pHrodo produced similar results (Fig. 6G and fig. S5). In line with our biochemical data in BV2 microglial cells as well as in HEK293 Flp-In cells, the AD risk variant p.R47H impaired phagocytosis to a much lesser extent in the bead uptake assay (Fig. 6F; **P = 0.004, Mann-Whitney U test) and was even normal for uptake of bacteria (Fig. 6G; n.s., P = 0.191, Mann-Whitney U test). Finally, we used the pathologically relevant amyloid β-peptide 1–42 ($A\beta_{1-42}$) as a substrate in the phagocytosis assays and demonstrated that TREM2 loss of function due to the missense mutations significantly impaired phagocytosis of $A\beta_{1-42}$ in three independent cell lines including BV2 microglial cells (Fig. 6H; ***P < 0.001, Mann-Whitney U test), HEK293 Flp-In cells (Fig. 6I; **P < 0.01, ***P < 0.001,

Table 2. Characteristics of patient and control study population used to measure plasma sTREM2. Data are expressed as number of patients (percent), mean ± SD, or median (IQR) as appropriate. Probability values (*P*) denote differences between control, AD, and FTD patient groups. χ^2 tests were used for gender. One-way ANOVA was used to compare age between groups followed by Tukey post hoc test. CSF biomarkers and sTREM2 were evaluated by nonparametric statistical analysis (Kruskal-Wallis and post hoc with Mann-Whitney *U* test).

Variable	Total (*n* = 172)	Controls (*n* = 86)	AD (*n* = 51)	FTD (*n* = 35)	*P*
Gender (F/M), no. (%)	103 (60)/69 (40)	55 (64)/31 (36)	36 (71)/15 (29)	12 (34)/23 (66)	0.002*
Age, years (mean ± SD)	64.1 ± 10.1	60.4 ± 9.5	70.7 ± 9.0	63.7 ± 8.4	<0.001†
CSF biomarkers					
$A\beta_{1-42}$ (pg/ml), median (IQR)	626.3 (453–813)	780.8 (645–902)	398.5 (301–508)	588.0 (478–824)	<0.001‡
T-tau (pg/ml), median (IQR)	244.4 (172–486)	202.8 (157–244)	675.0 (498–891)	230.1 (148–345)	<0.001§
P-tau_{181P} (pg/ml), median (IQR)	46.5 (36–74)	40.0 (34–49)	89.9 (73–103)	40.0 (28–53)	<0.001¶
sTREM2 (relative units)					
Median (IQR)	1.022 (0.703–1.590)	1.022 (0.675–1.864)	0.998 (0.702–1.375)	1.046 (0.759–1.399)	0.872

*Post hoc significances for gender: controls versus AD, $P = 0.427$; controls versus FTD, $P = 0.003$; AD versus FTD, $P = 0.001$. †Post hoc significances for age: controls versus AD, $P < 0.001$; controls versus FTD, $P = 0.165$; AD versus FTD, $P = 0.002$. ‡Post hoc significances for $A\beta_{1-42}$: controls versus AD, $P < 0.001$; controls versus FTD, $P < 0.001$; AD versus FTD, $P < 0.001$. §Post hoc significances for T-tau: controls versus AD, $P < 0.001$; controls versus FTD, $P = 0.054$; AD versus FTD, $P < 0.001$. ¶Post hoc significances for P-tau_{181P}: controls versus AD, $P < 0.001$; controls versus FTD, $P = 0.704$; AD versus FTD, $P < 0.001$.

Mann-Whitney *U* test), and $Trem2^{-/-}$ primary microglia (Fig. 6J; $^*P = 0.016$, $^{**}P < 0.01$, Mann-Whitney *U* test). Thus, mutations that severely reduce maturation of TREM2, such as p.T66M and p.Y38C, result in a significant loss of function of TREM2 as measured by three independent phagocytosis assays.

These findings suggest that expression of mature membrane-bound TREM2 correlates with phagocytic activity of microglia. Therefore, we reasoned that TREM2 may be modulated to increase clearance of cellular debris and amyloidogenic seeds. As proof of principle and as an additional link between cell surface TREM2 expression and phagocytosis, we investigated whether inhibition of TREM2 shedding, which increases cell surface TREM2 (Fig. 1, B and C), increases phagocytosis. In line with the data in Fig. 1, upon treatment of BV2 microglial cells endogenously expressing Trem2 (Fig. 4A), with a broad pharmacological inhibitor of ADAM proteases (GM 6001), proteolytic processing of endogenous Trem2 was significantly reduced (Fig. 7A; $^*P = 0.019$; n.s., $P > 0.05$, Mann-Whitney *U* test). Moreover, reduced Trem2 shedding correlated with a significant increase in phagocytosis as shown by increased uptake of *E. coli* (Fig. 7B; $^{***}P < 0.001$; n.s., $P > 0.05$, Mann-Whitney *U* test). Thus, these findings provide further evidence for a link between cell surface expression of Trem2 and phagocytosis.

DISCUSSION

Loss of function of TREM2 is associated with NHD—a rare recessive disorder characterized by early-onset dementia with clinical presentation similar to the behavioral variant of FTD (*1*). Recently, two independent genome-wide association studies linked missense variants in *TREM2* to an increased risk for developing late-onset AD (*4*, *5*). Subsequent studies confirmed the association in several AD cohorts (*27*, *28*) and further extended the finding to other neurodegenerative disorders including FTD (*6*, *8*, *9*), PD (*6*), and ALS (*7*). Although TREM2 variants are rare (population frequency ~0.3%), the effect size (odds ratio >3) is similar to that for APOEε4; in silico predictions suggest a probable damaging effect of the identified variants on TREM2 protein function (*4*, *8*). Biochemical and cell biological analyses of two FTD-associated TREM2 variants (p.Y38C and p.T66M) indicated misfolding of TREM2 followed by inhibition of cell surface transport (Figs. 2 to 4). Reduced surface exposure of TREM2 leads to impaired phagocytosis (Fig. 6), a finding that is consistent with a short hairpin RNA–mediated TREM2 knockdown phenotype (*14*). Whereas the FTD- and FTD-like–associated mutations, as well as the mutations of the conserved cysteine residues, displayed a very severe and consistent biochemical and functional phenotype, the AD-associated p.R47H mutation showed a much weaker effect on maturation, secretion, and phagocytic activity. Whether this is due to a weaker general effect of this TREM2 variant or rather a different cellular mechanism of action remains to be investigated. Notably, the p.R47H mutation is considered to be a risk factor for AD (*4*, *5*), whereas the other investigated variants are causative mutations when in the homozygous state (*2*). Furthermore, we observed that the TREM2 p.R47H mutant is expressed at lower rates, suggesting that this variant may be unstable and prone to degradation.

Our data suggest that reduced TREM2 function impairs phagocytosis, which may contribute to neurodegeneration through different mechanisms. First, reduced phagocytosis may prevent engulfment of cellular debris, which could result in a chronic inflammatory response (*12*). Second, amyloidogenic seeds, which are thought to prime neurodegeneration (*29*), may also be eliminated in a TREM2-dependent manner. Third, in the case of AD, TREM2 is up-regulated around amyloid plaques (*4*, *30*), and it is tempting to speculate that this reflects a defense mechanism to remove unwanted protein aggregates. In line with this hypothesis, phagocytosis assays using preaggregated $A\beta_{1-42}$ as a ligand suggest that TREM2 is indeed capable of removing amyloidogenic protein aggregates (Fig. 6, H to J). Finally, ER retention of mutant TREM2 may also cause ER stress, which could affect function and survival of microglia specifically in the case of the p.T66M and p.Y38C mutations.

TREM2 is a type I transmembrane glycoprotein that has been shown to shuttle to and from the plasma membrane in microglial cells upon cell stimulation by ionomycin or interferon-γ (*31*). Cell surface expression of TREM2 can be regulated by either phagocytic receptor recycling (*23*) or ectodomain shedding (Figs. 1, 4, and 7) during which sTREM2 fragments are released from the cell. Whether sTREM2 has a paracrine signaling

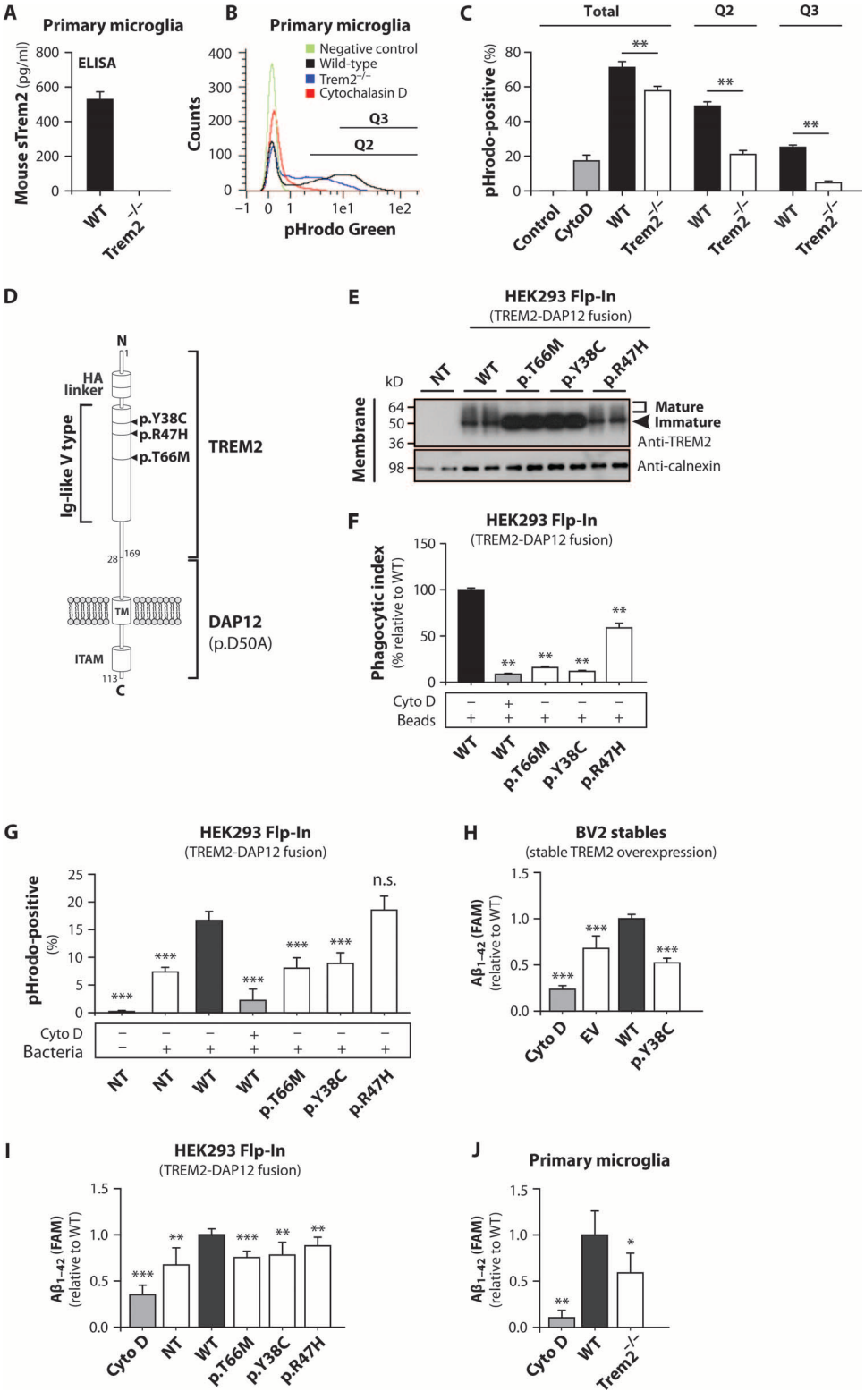

Fig. 6. Impaired phagocytosis in microglia expressing mutant TREM2. (**A**) ELISA-based analysis of sTrem2 in the supernatants of WT or Trem2 knockout (Trem2$^{-/-}$) primary microglia. (**B** and **C**) Flow cytometric analysis of the phagocytic capacity of primary microglia using pHrodo *E. coli* as target particles. Q2, 50th percentile; Q3, 75th percentile. (**D**) Illustration of TREM2-DAP12 fusion construct (*25*) used in the phagocytosis assays shown in (F), (G), and (I). ITAM, immunoreceptor tyrosine-based activation motif. (**E**) Anti-TREM2 immunoblot of TREM2-DAP12–expressing HEK293 Flp-In cells. Anti-calnexin antibody was used as a loading control. (**F**) Phagocytosis of fluorescently labeled latex beads in HEK293 Flp-In cells stably expressing TREM2-DAP12 fusion constructs. Phagocytic index (percentage of cells that phagocytose beads expressed relative to WT) from three independent experiments is shown as mean ± SD. (**G**) Phagocytosis of pHrodo *E. coli* in HEK293 Flp-In cells stably expressing TREM2-DAP12 fusion constructs and quantified by flow cytometry. Data are depicted as means ± SD from at least two independent experiments. (**H** to **J**) Phagocytosis of 6-carboxyfluorescein (FAM)–labeled $A\beta_{1–42}$ by (H) BV2 cells stably expressing WT or mutant TREM2, (I) HEK293 Flp-In cells stably expressing TREM2-DAP12 fusion constructs, and (J) primary microglia derived from Trem2$^{-/-}$ mice is shown as mean ± SD from two independent experiments (J) or three independent experiments (H and I) and is expressed relative to WT controls. In all assays, cytochalasin D (10 μM) was used as a negative control to inhibit phagocytosis. Statistical differences were calculated by Mann-Whitney *U* test. $^{*}P < 0.05$; $^{**}P < 0.01$; $^{***}P \leq 0.001$.

function or serves as a competitor for TREM2 ligands, as is the case for TREM1 (*12*), remains unclear. However, such functions would also be compromised by the reduced secretion of TREM2 variants investigated here. sTREM2 can be readily detected by ELISA-based methods (*16*) and could therefore serve as a possible marker for neurodegenerative disorders in the future, although further validation in additional patient cohorts is needed. A patient with an FTD-like syndrome associated with the p.T66M mutation showed no sTREM2 in either CSF or plasma. Consistent with a loss of function of TREM2, homozygous *DAP12* deletions are also found in patients with NHD (*1*, *32*). If these results are confirmed in a much larger sample of patients, sTREM2 concentrations in CSF potentially could be used to screen for TREM2 homozygous missense mutations in an analogous way to progranulin mutation carrier screening (*33*–*35*). Furthermore, in a cross-sectional analysis of sTREM2 concentrations in CSF of FTD patients, we found significantly reduced concentrations of sTREM2 in FTD patients

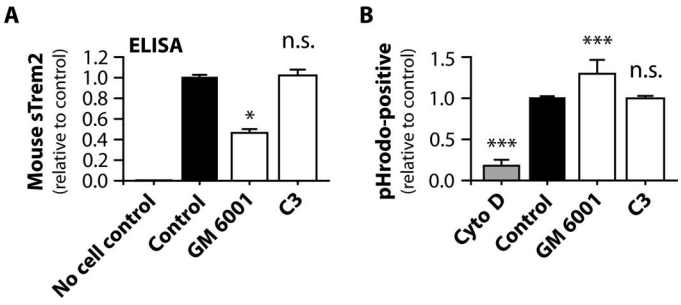

Fig. 7. Pharmacological inhibition of ADAM proteases decreased endogenous sTrem2 and increased phagocytosis in BV2 cells. (**A**) Endogenous sTrem2 in supernatants from BV2 cells after inhibition of ADAM proteases (GM 6001) or BACE1 (C3). (**B**) Phagocytosis of pHrodo *E. coli* in BV2 cells treated with GM 6001 or C3. Data are represented as means ± SD from at least two independent experiments and expressed relative to non-treated control; $n = 4$ (A) and $n = 7$ to 9 (B). Statistical differences were calculated by Mann-Whitney *U* test. $^*P < 0.05$; $^{***}P < 0.001$.

compared to neurologically normal controls, further supporting a TREM2 loss-of-function mechanism in the pathogenesis of AD and FTD. Although the overlap between groups precludes the current utilization of sTREM2 in clinical settings, we believe that CSF sTREM2 deserves further research as a potential marker for neurodegenerative diseases, probably in combination with other yet to be identified markers. Finally, our findings suggest that TREM2-dependent phagocytosis could be modulated, hence opening the door for new therapeutic strategies. Indeed, as a proof of principle, we showed that this can be achieved by blocking ADAM proteases (Fig. 7). However, therapeutic application would require a search for compounds that selectively and specifically enhance TREM2 activity without interfering with the expression of other proteins or essential signaling pathways.

MATERIALS AND METHODS

Study design

The first part of this study was designed to determine whether TREM2 missense mutations, which recently have been identified as risk factor for several neurodegenerative diseases, alter maturation and processing of TREM2 and ultimately cause a loss of TREM2 protein function. We investigated TREM2 processing and function using several cell lines including HEK293 Flp-In cells, microglial cell lines (BV2 cells), and primary microglial cells derived from $Trem2^{-/-}$ mice. The second aim was to study the sTREM2 concentrations in CSF and plasma of patients diagnosed with FTD-like syndrome, FTD, or AD and compare them to those of healthy controls. For these purposes, we performed a cross-sectional study in which we measured sTREM2 in CSF and plasma samples from six specialized neurological referral centers. We studied all samples available from these centers; we did not perform a priori calculation of sample size. Clinical diagnoses were made according to internationally accepted criteria. In the final analysis, we excluded those control individuals and FTD patients who had an AD CSF profile defined by the Mattsson *et al.* equation (*36*), and, conversely, we excluded those clinically diagnosed AD patients who did not have an AD CSF profile. sTREM2 measurements were performed in an ELISA-based assay that we developed. The measurements were made in a blinded fashion. To study the consequences of TREM2 loss of function, we performed phagocytosis assays using three independent targets (latex beads, *E. coli* bacteria, and $A\beta_{1-42}$) and finally studied whether modulation of TREM2 could alter microglial function.

Cell culture and generation of isogenic cell lines

Flp-In 293 cells (HEK293 Flp-In; Life Technologies) were cultured in Dulbecco's modified Eagle's medium (DMEM) with Glutamax I, supplemented with 10% (v/v) fetal calf serum (FCS), Zeocin (200 μg/ml), and penicillin/streptomycin (PAA Laboratories). Transfections of complementary DNA (cDNA) constructs were carried out using Lipofectamine LTX with Plus Reagent according to the manufacturer's recommendations. For stable overexpression of human TREM2 cDNA constructs, HEK293 Flp-In cells were cotransfected with the TREM2 cDNA constructs and pOG44 (Flp-recombinase expression vector; Life Technologies) and selected using hygromycin B (200 μg/ml). BV2 microglia cells (*21*) were cultured in DMEM with Glutamax I, supplemented with 10% (v/v) FCS and penicillin/streptomycin, and stable TREM2-expressing cell lines were selected using Zeocin (200 μg/ml). Cell lines were regularly monitored for *Mycoplasma* contamination via a PCR-based method, and all results were negative throughout the course of the study. If not stated otherwise, products for cell culture experiments were obtained from Life Technologies.

Primary microglia cell culture

Primary microglia were isolated from postnatal day P5 to P6 mouse brains using MACS Technology (Miltenyi Biotec) according to the manufacturer's instructions. Briefly, brain cortices were dissected, freed from meninges, and dissociated by enzymatic digestion using a Neural Tissue Dissociation Kit P. CD11b-positive microglia were magnetically labeled using CD11b MicroBeads, loaded onto a MACS column, and subjected to magnetic separation. Isolated microglia were plated onto 24-well plate at a density of 8.5×10^4 cells per well and cultured in DMEM/F12 medium (Life Technologies) supplemented with 10% heat-inactivated FCS (Sigma) and 1% penicillin/streptomycin and maintained in a humidified 5% CO_2 incubator at 37°C. After 24 hours, cultured medium was replaced with fresh medium for 2 to 4 days until use for phagocytosis assays.

Phagocytosis assays

Bead uptake assays using HEK293 Flp-In cells stably expressing either wild-type or mutant TREM2-DAP12 fusion constructs (*25*) were performed essentially as described before (*23*). Briefly, cells were plated in 24-well plates at a density of 5×10^4 cells and cultured overnight. Preopsonized [50% FCS in phosphate-buffered saline (PBS)] latex beads (6 μm, internally dyed with the fluorophore Flash Red; Polysciences Inc.) were added to the cells at a concentration of 20 beads per cell and incubated for 90 min at 37°C. As a negative control, phagocytosis was inhibited with 10 μM cytochalasin D 30 min before addition of latex beads. Cells were harvested using TrypLE buffer (Life Technologies), washed three times with fluorescence-activated cell sorting (FACS) sample buffer (1% FCS and 0.02% sodium azide in PBS), and analyzed by flow cytometry on a FACSCalibur flow cytometer (BD Biosciences). Data analysis was performed using FlowJo version 9.7.1.

Phagocytosis of fluorogenic *E. coli* particles (pHrodo Green, Molecular Probes) was analyzed using BV2 microglial cells, primary microglia or HEK293 Flp-In cells stably expressing either wild-type or mutant TREM2-DAP12 fusion constructs (*25*). Briefly, cells were plated in 24-well plates at a density of 2×10^5 (HEK293 Flp-In), 1×10^5 (BV2), or 8.5×10^4 (primary

microglia) cells and cultured for 24 to 48 hours. pHrodo *E. coli* bioparticles were dissolved in PBS to a concentration of 1 μg/μl, and a total of 50 μg of bioparticles was added per condition and incubated for 60 min at 37°C. As a negative control, phagocytosis was inhibited with 10 μM cytochalasin D, which was added 30 min before addition of pHrodo *E. coli* bioparticles. Cells were harvested by trypsinization, washed two times with FACS sample buffer, and analyzed by flow cytometry on a MACSQuant VYB flow cytometer (Miltenyi Biotec). Data analysis was performed using the MACSQuantify software (Miltenyi Biotec).

Phagocytosis of aggregated FAM-labeled $A\beta_{1-42}$ (Anaspec) was analyzed similar to previously described methods (*37*). Briefly, FAM-labeled $A\beta_{1-42}$ was aggregated overnight at 37°C with agitation. Primary microglia, BV2, or HEK293 Flp-In cells were plated at 2×10^4, 1.5×10^4, 5×10^4 cells per well, respectively, in poly-L-lysine–coated black-walled 96-well plates (Greiner Bio One) and cultured overnight. Aβ was added to a final concentration of 0.5 μM (primary microglia) or 1.5 μM (HEK293 Flp-In and BV2) and incubated for 4 hours at 37°C. Extracellular $A\beta_{1-42}$ was quenched with 100 μl of 0.2% trypan blue in PBS (pH 4.4) for 1 min. After aspiration, fluorescence was measured at 485-nm excitation/538-nm emission using a Fluoroskan Ascent FL plate reader (Labsystems).

Patient material

CSF samples were obtained by lumbar puncture following standard procedures, collected in polypropylene tubes, and immediately frozen at −80°C until use (*36*, *38*). Six specialized neurological referral centers were involved in the study. AD was diagnosed according to the National Institute of Neurological and Communicative Disorders and Stroke and the Alzheimer's Disease and Related Disorders Association criteria (*39*). For patients recruited before 2011, FTD was diagnosed according to the Neary consensus criteria (*40*). Thereafter, patients diagnosed of bvFTD (behavioral variant FTD) followed the new revised bvFTD criteria (*41*), and those with semantic dementia or progressive nonfluent aphasia fulfilled the primary progressive aphasia international consensus criteria (*42*). The control group (n = 88) consisted of individuals fulfilling the following inclusion criteria: (i) no neurological or psychiatric antecedents, (ii) no organic disease involving the central nervous system after extensive clinical examination, and (iii) cognitive deterioration was ruled out after evaluation by a neurologist with experience in neurodegenerative dementias. Among them, there were two patients who were diagnosed with disorders of the peripheral nervous system and two with depression. To improve the accuracy of the diagnosis, we excluded those control individuals (6 of 94, 6.4%) and clinically diagnosed FTD patients (7 of 57, 12.3%) who had an AD CSF profile defined by the Mattsson *et al.* equation (*36*) [$(A\beta_{42}$/P-tau)/(3.694 + 0.0105 × T-tau)], and, conversely, we excluded those clinically diagnosed AD patients who did not have an AD CSF profile following the former equation (24 of 80, 30%). The decrease in sTREM2 concentrations in AD and FTD patients compared to control individuals was observed both including and excluding those patients. Among the FTD group, two patients carried a C9orf72 repeat expansion and three subjects carried a progranulin (GRN) mutation. Again, the decrease in sTREM2 concentrations in FTD patients compared to control individuals was observed both including and excluding the genetic cases from the FTD group. All patients gave written informed consent, and the study was approved by the local ethics committees of the participating centers.

sTREM2 ELISA

To quantify the concentrations of sTREM2 in human CSF, EDTA-plasma samples, or cell culture supernatants, an ELISA for human sTREM2 was established using the Meso Scale Discovery SECTOR Imager 2400 similarly to previously established ELISAs (*43*). Streptavidin-coated 96-well plates were blocked overnight at 4°C in blocking buffer [0.5% bovine serum albumin (BSA) and 0.05% Tween 20 in PBS (pH 7.4)]. For the detection of human sTREM2, plates were incubated for 1 hour at room temperature with biotinylated polyclonal goat anti-human TREM2 capture antibody (0.25 μg/ml) (R&D Systems) diluted in blocking buffer. Plates were washed subsequently for four times with washing buffer (0.05% Tween 20 in PBS) and incubated for 2 hours at room temperature with samples diluted 1:4 in assay buffer [0.25% BSA and 0.05% Tween 20 in PBS (pH 7.4)] supplemented with protease inhibitors (Sigma). A recombinant human TREM2 protein (Hölzel Diagnostika) was diluted in assay buffer in a twofold serial dilution and used for the standard curve (concentration range, 4000 to 62.5 pg/ml). Plates were washed three times for 5 min with washing buffer before incubation for 1 hour at room temperature with mouse monoclonal anti-TREM2 antibody (1 μg/ml) (Santa Cruz Biotechnology; B-3) diluted in blocking buffer. After three additional washing steps, plates were incubated with a SULFO-TAG–labeled anti-mouse secondary antibody (1:1000; Meso Scale Discovery) and incubated for 1 hour in the dark. Last, plates were washed three times with wash buffer followed by two washing steps in PBS and developed by adding Meso Scale Discovery Read buffer. The light emission at 620 nm after electrochemical stimulation was measured using the Meso Scale Discovery SECTOR Imager 2400 reader.

Spike recovery, linearity, interplate, and interday variability for the human sTREM2 ELISA was determined using both a dedicated CSF and plasma sample (tables S2 and S3). Repeated freeze-thaw cycles had only minimal effects on sTREM2 concentrations in CSF (fig. S4C) and no effect on sTREM2 concentrations in plasma (fig. S4D). The specificity of the used ELISA system was further validated by anti-TREM2 immunoblotting showing high degree of correlation between the ELISA readings and immunoreactivity on the immunoblot using an independent anti-TREM2 antibody (fig. S4F).

To measure murine sTREM2, the same procedure as outlined above was followed using biotinylated polyclonal sheep anti-mouse TREM2 (0.25 μg/ml) as capture antibody, rat monoclonal anti-mouse TREM2 (1 μg/ml) as detection antibody (both R&D Systems), and a SULFO-TAG–labeled goat anti-rat secondary antibody (1:1000; Meso Scale Discovery) as secondary antibody. As standard, a recombinant mouse TREM2 protein (Hölzel Diagnostika) was used.

To quantify the levels of sTREM2 secreted from HEK293 Flp-In or BV2 cells, conditioned media from biological replicates, collected as described above, were analyzed in duplicates using either a commercial TREM2 ELISA according to the manufacturer's recommendations (Sino Biological; Figs. 1B and 2B) or our newly established human (Fig. 4, A and B) or mouse (Fig. 7, A and B) sTREM2 ELISA. The sTREM2 standard curves were generated using the MasterPlex ReaderFit software (MiraiBio Group, Hitachi Solutions America) through a five-parameter logistic fit.

Statistical analysis

The χ^2 test was used to compare differences in categorical variables. One-way ANOVA followed by Tukey post hoc test was used to compare normally distributed continuous variables. Data that did not follow a normal distribution (including sTREM2 concentrations in CSF and plasma) were analyzed with nonparametric tests (Kruskal-Wallis followed by post hoc Mann-Whitney U test). To control for the effect

of potential confounders (gender, age, and center origin of the sample) on sTREM2 in CSF, we log-transformed this variable to achieve a normal distribution, and performed an ANCOVA. Statistical significance was set to 5% ($\alpha = 0.05$). All tests were two-sided, and all data were analyzed using the Statistical Package for the Social Sciences 20.0 (SPSS Inc.).

SUPPLEMENTARY MATERIALS

www.sciencetranslationalmedicine.org/cgi/content/full/6/243/243ra86/DC1
Materials and Methods
Fig. S1. Absence of TREM2 fragments containing C-terminal FLAG tag.
Fig. S2. Analysis of maturation of TREM2.
Fig. S3. Characterization of BV2 cells stably overexpressing human TREM2.
Fig. S4. Characterization of novel sTREM2 ELISA.
Fig. S5. Impaired phagocytosis by mutant TREM2.
Table S1. Primers used for RT-PCR analysis.
Table S2. Characterization of novel sTREM2 ELISA.
Table S3. Spike recovery and linearity test for CSF and plasma sTREM2 ELISA.
References (*44*–*48*)

REFERENCES AND NOTES

1. H. H. Klünemann, B. H. Ridha, L. Magy, J. R. Wherrett, D. M. Hemelsoet, R. W. Keen, J. L. De Bleecker, M. N. Rossor, J. Marienhagen, H. E. Klein, L. Peltonen, J. Paloneva, The genetic causes of basal ganglia calcification, dementia, and bone cysts: *DAP12* and *TREM2*. *Neurology* **64**, 1502–1507 (2005).
2. R. J. Guerreiro, E. Lohmann, J. M. Brás, J. R. Gibbs, J. D. Rohrer, N. Gurunlian, B. Dursun, B. Bilgic, H. Hanagasi, H. Gurvit, M. Emre, A. Singleton, J. Hardy, Using exome sequencing to reveal mutations in *TREM2* presenting as a frontotemporal dementia-like syndrome without bone involvement. *JAMA Neurol.* **70**, 78–84 (2013).
3. R. Guerreiro, B. Bilgic, G. Guven, J. Brás, J. Rohrer, E. Lohmann, H. Hanagasi, H. Gurvit, M. Emre, Novel compound heterozygous mutation in *TREM2* found in a Turkish frontotemporal dementia-like family. *Neurobiol. Aging* **34**, 2890.e1–2890.e5 (2013).
4. R. Guerreiro, A. Wojtas, J. Bras, M. Carrasquillo, E. Rogaeva, E. Majounie, C. Cruchaga, C. Sassi, J. S. Kauwe, S. Younkin, L. Hazrati, J. Collinge, J. Pocock, T. Lashley, J. Williams, J. C. Lambert, P. Amouyel, A. Goate, R. Rademakers, K. Morgan, J. Powell, P. St George-Hyslop, A. Singleton, J. Hardy; Alzheimer Genetic Analysis Group, *TREM2* variants in Alzheimer's disease. *N. Engl. J. Med.* **368**, 117–127 (2013).
5. T. Jonsson, H. Stefansson, S. Steinberg, I. Jonsdottir, P. V. Jonsson, J. Snaedal, S. Bjornsson, J. Huttenlocher, A. I. Levey, J. J. Lah, D. Rujescu, H. Hampel, I. Giegling, O. A. Andreassen, K. Engedal, I. Ulstein, S. Djurovic, C. Ibrahim-Verbaas, A. Hofman, M. A. Ikram, C. M. van Duijn, U. Thorsteinsdottir, A. Kong, K. Stefansson, Variant of *TREM2* associated with the risk of Alzheimer's disease. *N. Engl. J. Med.* **368**, 107–116 (2013).
6. S. Rayaprolu, B. Mullen, M. Baker, T. Lynch, E. Finger, W. W. Seeley, K. J. Hatanpaa, C. Lomen-Hoerth, A. Kertesz, E. H. Bigio, C. Lippa, K. A. Josephs, D. S. Knopman, C. L. White III, R. Caselli, I. R. Mackenzie, B. L. Miller, M. Boczarska-Jedynak, G. Opala, A. Krygowska-Wajs, M. Barcikowska, S. G. Younkin, R. C. Petersen, N. Ertekin-Taner, R. J. Uitti, J. F. Meschia, K. B. Boylan, B. F. Boeve, N. R. Graff-Radford, Z. K. Wszolek, D. W. Dickson, R. Rademakers, O. A. Ross, TREM2 in neurodegeneration: Evidence for association of the p.R47H variant with frontotemporal dementia and Parkinson's disease. *Mol. Neurodegener.* **8**, 19 (2013).
7. J. Cady, E. D. Koval, B. A. Benitez, C. Zaidman, J. Jockel-Balsarotti, P. Allred, R. H. Baloh, J. Ravits, E. Simpson, S. H. Appel, A. Pestronk, A. M. Goate, T. M. Miller, C. Cruchaga, M. B. Harms, *TREM2* variant p.R47H as a risk factor for sporadic amyotrophic lateral sclerosis. *JAMA Neurol.* **71**, 449–453 (2014).
8. E. Cuyvers, K. Bettens, S. Philtjens, T. Van Langenhove, I. Gijselinck, J. van der Zee, S. Engelborghs, M. Vandenbulcke, J. Van Dongen, N. Geerts, G. Maes, M. Mattheijssens, K. Peeters, P. Cras, R. Vandenberghe, P. P. De Deyn, C. Van Broeckhoven, M. Cruts, K. Sleegers; BELNEU consortium, Investigating the role of rare heterozygous *TREM2* variants in Alzheimer's disease and frontotemporal dementia. *Neurobiol. Aging* **35**, 726.e11–726.e19 (2014).
9. B. Borroni, F. Ferrari, D. Galimberti, B. Nacmias, C. Barone, S. Bagnoli, C. Fenoglio, I. Piaceri, S. Archetti, C. Bonvicini, M. Gennarelli, M. Turla, E. Scarpini, S. Sorbi, A. Padovani, Heterozygous *TREM2* mutations in frontotemporal dementia. *Neurobiol. Aging* **35**, 934.e7–934.e10 (2014).
10. P. Forabosco, A. Ramasamy, D. Trabzuni, R. Walker, C. Smith, J. Bras, A. P. Levine, J. Hardy, J. M. Pocock, R. Guerreiro, M. E. Weale, M. Ryten, Insights into *TREM2* biology by network analysis of human brain gene expression data. *Neurobiol. Aging* **34**, 2699–2714 (2013).
11. C. L. Hsieh, M. Koike, S. C. Spusta, E. C. Niemi, M. Yenari, M. C. Nakamura, W. E. Seaman, A role for TREM2 ligands in the phagocytosis of apoptotic neuronal cells by microglia. *J. Neurochem.* **109**, 1144–1156 (2009).
12. J. Klesney-Tait, I. R. Turnbull, M. Colonna, The TREM receptor family and signal integration. *Nat. Immunol.* **7**, 1266–1273 (2006).
13. J. W. Ford, D. W. McVicar, TREM and TREM-like receptors in inflammation and disease. *Curr. Opin. Immunol.* **21**, 38–46 (2009).
14. K. Takahashi, C. D. Rochford, H. Neumann, Clearance of apoptotic neurons without inflammation by microglial triggering receptor expressed on myeloid cells-2. *J. Exp. Med.* **201**, 647–657 (2005).
15. S. Gibot, M. N. Kolopp-Sarda, M. C. Béné, P. E. Bollaert, A. Lozniewski, F. Mory, B. Levy, G. C. Faure, A soluble form of the triggering receptor expressed on myeloid cells-1 modulates the inflammatory response in murine sepsis. *J. Exp. Med.* **200**, 1419–1426 (2004).
16. L. Piccio, C. Buonsanti, M. Cella, I. Tassi, R. E. Schmidt, C. Fenoglio, J. Rinker II, R. T. Naismith, P. Panina-Bordignon, N. Passini, D. Galimberti, E. Scarpini, M. Colonna, A. H. Cross, Identification of soluble TREM-2 in the cerebrospinal fluid and its association with multiple sclerosis and CNS inflammation. *Brain* **131**, 3081–3091 (2008).
17. P. Wunderlich, K. Glebov, N. Kemmerling, N. T. Tien, H. Neumann, J. Walter, Sequential proteolytic processing of the triggering receptor expressed on myeloid cells-2 (TREM2) protein by ectodomain shedding and γ-secretase-dependent intramembranous cleavage. *J. Biol. Chem.* **288**, 33027–33036 (2013).
18. S. F. Lichtenthaler, C. Haass, H. Steiner, Regulated intramembrane proteolysis—Lessons from amyloid precursor protein processing. *J. Neurochem.* **117**, 779–796 (2011).
19. R. Fluhrer, H. Steiner, C. Haass, Intramembrane proteolysis by signal peptide peptidases: A comparative discussion of GXGD-type aspartyl proteases. *J. Biol. Chem.* **284**, 13975–13979 (2009).
20. M. Colonna, TREMs in the immune system and beyond. *Nat. Rev. Immunol.* **3**, 445–453 (2003).
21. V. Bocchini, R. Mazzolla, R. Barluzzi, E. Blasi, P. Sick, H. Kettenmann, An immortalized cell line expresses properties of activated microglial cells. *J. Neurosci. Res.* **31**, 616–621 (1992).
22. B. Stansley, J. Post, K. Hensley, A comparative review of cell culture systems for the study of microglial biology in Alzheimer's disease. *J. Neuroinflammation* **9**, 115 (2012).
23. K. M. Lucin, C. E. O'Brien, G. Bieri, E. Czirr, K. I. Mosher, R. J. Abbey, D. F. Mastroeni, J. Rogers, B. Spencer, E. Masliah, T. Wyss-Coray, Microglial beclin 1 regulates retromer trafficking and phagocytosis and is impaired in Alzheimer's disease. *Neuron* **79**, 873–886 (2013).
24. I. R. Turnbull, S. Gilfillan, M. Cella, T. Aoshi, M. Miller, L. Piccio, M. Hernandez, M. Colonna, Cutting edge: TREM-2 attenuates macrophage activation. *J. Immunol.* **177**, 3520–3524 (2006).
25. J. A. Hamerman, J. R. Jarjoura, M. B. Humphrey, M. C. Nakamura, W. E. Seaman, L. L. Lanier, Cutting edge: Inhibition of TLR and FcR responses in macrophages by triggering receptor expressed on myeloid cells (TREM)-2 and DAP12. *J. Immunol.* **177**, 2051–2055 (2006).
26. E. N. N'Diaye, C. S. Branda, S. S. Branda, L. Nevarez, M. Colonna, C. Lowell, J. A. Hamerman, W. E. Seaman, TREM-2 (triggering receptor expressed on myeloid cells 2) is a phagocytic receptor for bacteria. *J. Cell Biol.* **184**, 215–223 (2009).
27. B. A. Benitez, B. Cooper, P. Pastor, S. C. Jin, E. Lorenzo, S. Cervantes, C. Cruchaga, *TREM2* is associated with the risk of Alzheimer's disease in Spanish population. *Neurobiol. Aging* **34**, 1711.e15–1711.e17 (2013).
28. C. Pottier, D. Wallon, S. Rousseau, A. Rovelet-Lecrux, A. C. Richard, A. Rollin-Sillaire, T. Frebourg, D. Campion, D. Hannequin, TREM2 R47H variant as a risk factor for early-onset Alzheimer's disease. *J. Alzheimers Dis.* **35**, 45–49 (2013).
29. M. Jucker, L. C. Walker, Self-propagation of pathogenic protein aggregates in neurodegenerative diseases. *Nature* **501**, 45–51 (2013).
30. B. Melchior, A. E. Garcia, B. K. Hsiung, K. M. Lo, J. M. Doose, J. C. Thrash, A. K. Stalder, M. Staufenbiel, H. Neumann, M. J. Carson, Dual induction of TREM2 and tolerance-related transcript, Tmem176b, in amyloid transgenic mice: Implications for vaccine-based therapies for Alzheimer's disease. *ASN Neuro.* **2**, e00037 (2010).
31. I. Prada, G. N. Ongania, C. Buonsanti, P. Panina-Bordignon, J. Meldolesi, Triggering receptor expressed in myeloid cells 2 (TREM2) trafficking in microglial cells: Continuous shuttling to and from the plasma membrane regulated by cell stimulation. *Neuroscience* **140**, 1139–1148 (2006).
32. T. Kondo, K. Takahashi, N. Kohara, Y. Takahashi, S. Hayashi, H. Takahashi, H. Matsuo, M. Yamazaki, K. Inoue, K. Miyamoto, T. Yamamura, Heterogeneity of presenile dementia with bone cysts (Nasu–Hakola disease): Three genetic forms. *Neurology* **59**, 1105–1107 (2002).
33. N. Finch, M. Baker, R. Crook, K. Swanson, K. Kuntz, R. Surtees, G. Bisceglio, A. Rovelet-Lecrux, B. Boeve, R. C. Petersen, D. W. Dickson, S. G. Younkin, V. Deramecourt, J. Crook, N. R. Graff-Radford, R. Rademakers, Plasma progranulin levels predict progranulin mutation status in frontotemporal dementia patients and asymptomatic family members. *Brain* **132**, 583–591 (2009).
34. A. Antonell, S. Gil, R. Sánchez-Valle, M. Balasa, B. Bosch, M. C. Prat, A. C. Chiollaz, M. Fernández, J. Yagüe, J. L. Molinuevo, A. Lladó, Serum progranulin levels in patients with frontotemporal lobar degeneration and Alzheimer's disease: Detection of GRN mutations in a Spanish cohort. *J. Alzheimers Dis.* **31**, 581–591 (2012).
35. K. Sleegers, N. Brouwers, C. Van Broeckhoven, Role of progranulin as a biomarker for Alzheimer's disease. *Biomarkers Med.* **4**, 37–50 (2010).

36. N. Mattsson, H. Zetterberg, O. Hansson, N. Andreasen, L. Parnetti, M. Jonsson, S. K. Herukka, W. M. van der Flier, M. A. Blankenstein, M. Ewers, K. Rich, E. Kaiser, M. Verbeek, M. Tsolaki, E. Mulugeta, E. Rosén, D. Aarsland, P. J. Visser, J. Schröder, J. Marcusson, M. de Leon, H. Hampel, P. Scheltens, T. Pirttilä, A. Wallin, M. E. Jönhagen, L. Minthon, B. Winblad, K. Blennow, CSF biomarkers and incipient Alzheimer disease in patients with mild cognitive impairment. *JAMA* **302**, 385–393 (2009).
37. S. Fleisher-Berkovich, T. Filipovich-Rimon, S. Ben-Shmuel, C. Hulsmann, M. P. Kummer, M. T. Heneka, Distinct modulation of microglial amyloid β phagocytosis and migration by neuropeptides. *J. Neuroinflammation* **7**, 61 (2010).
38. S. Engelborghs, K. De Vreese, T. Van de Casteele, H. Vanderstichele, B. Van Everbroeck, P. Cras, J. J. Martin, E. Vanmechelen, P. P. De Deyn, Diagnostic performance of a CSF-biomarker panel in autopsy-confirmed dementia. *Neurobiol. Aging* **29**, 1143–1159 (2008).
39. G. McKhann, D. Drachman, M. Folstein, R. Katzman, D. Price, E. M. Stadlan, Clinical diagnosis of Alzheimer's disease: Report of the NINCDS-ADRDA Work Group under the auspices of Department of Health and Human Services Task Force on Alzheimer's Disease. *Neurology* **34**, 939–944 (1984).
40. D. Neary, J. S. Snowden, L. Gustafson, U. Passant, D. Stuss, S. Black, M. Freedman, A. Kertesz, P. H. Robert, M. Albert, K. Boone, B. L. Miller, J. Cummings, D. F. Benson, Frontotemporal lobar degeneration: A consensus on clinical diagnostic criteria. *Neurology* **51**, 1546–1554 (1998).
41. K. Rascovsky, J. R. Hodges, D. Knopman, M. F. Mendez, J. H. Kramer, J. Neuhaus, J. C. van Swieten, H. Seelaar, E. G. Dopper, C. U. Onyike, A. E. Hillis, K. A. Josephs, B. F. Boeve, A. Kertesz, W. W. Seeley, K. P. Rankin, J. K. Johnson, M. L. Gorno-Tempini, H. Rosen, C. E. Prioleau-Latham, A. Lee, C. M. Kipps, P. Lillo, O. Piguet, J. D. Rohrer, M. N. Rossor, J. D. Warren, N. C. Fox, D. Galasko, D. P. Salmon, S. E. Black, M. Mesulam, S. Weintraub, B. C. Dickerson, J. Diehl-Schmid, F. Pasquier, V. Deramecourt, F. Lebert, Y. Pijnenburg, T. W. Chow, F. Manes, J. Grafman, S. F. Cappa, M. Freedman, M. Grossman, B. L. Miller, Sensitivity of revised diagnostic criteria for the behavioural variant of frontotemporal dementia. *Brain* **134**, 2456–2477 (2011).
42. M. L. Gorno-Tempini, A. E. Hillis, S. Weintraub, A. Kertesz, M. Mendez, S. F. Cappa, J. M. Ogar, J. D. Rohrer, S. Black, B. F. Boeve, F. Manes, N. F. Dronkers, R. Vandenberghe, K. Rascovsky, K. Patterson, B. L. Miller, D. S. Knopman, J. R. Hodges, M. M. Mesulam, M. Grossman, Classification of primary progressive aphasia and its variants. *Neurology* **76**, 1006–1014 (2011).
43. A. Capell, S. Liebscher, K. Fellerer, N. Brouwers, M. Willem, S. Lammich, I. Gijselinck, T. Bittner, A. M. Carlson, F. Sasse, B. Kunze, H. Steinmetz, R. Jansen, D. Dormann, K. Sleegers, M. Cruts, J. Herms, C. Van Broeckhoven, C. Haass, Rescue of progranulin deficiency associated with frontotemporal lobar degeneration by alkalizing reagents and inhibition of vacuolar ATPase. *J. Neurosci.* **31**, 1885–1894 (2011).
44. D. Fleck, F. van Bebber, A. Colombo, C. Galante, B. M. Schwenk, L. Rabe, H. Hampel, B. Novak, E. Kremmer, S. Tahirovic, D. Edbauer, S. F. Lichtenthaler, B. Schmid, M. Willem, C. Haass, Dual cleavage of neuregulin 1 type III by BACE1 and ADAM17 liberates its EGF-like domain and allows paracrine signaling. *J. Neurosci.* **33**, 7856–7869 (2013).
45. A. Ludwig, C. Hundhausen, M. H. Lambert, N. Broadway, R. C. Andrews, D. M. Bickett, M. A. Leesnitzer, J. D. Becherer, Metalloproteinase inhibitors for the disintegrin-like metalloproteinases ADAM10 and ADAM17 that differentially block constitutive and phorbol ester-inducible shedding of cell surface molecules. *Comb. Chem. High Throughput Screen.* **8**, 161–171 (2005).
46. M. Willem, A. N. Garratt, B. Novak, M. Citron, S. Kaufmann, A. Rittger, B. DeStrooper, P. Saftig, C. Birchmeier, C. Haass, Control of peripheral nerve myelination by the β-secretase BACE1. *Science* **314**, 664–666 (2006).
47. C. Haass, A. Y. Hung, D. J. Selkoe, Processing of β-amyloid precursor protein in microglia and astrocytes favors an internal localization over constitutive secretion. *J. Neurosci.* **11**, 3783–3793 (1991).
48. C. M. Lang, K. Fellerer, B. M. Schwenk, P. H. Kuhn, E. Kremmer, D. Edbauer, A. Capell, C. Haass, Membrane orientation and subcellular localization of transmembrane protein 106B (TMEM106B), a major risk factor for frontotemporal lobar degeneration. *J. Biol. Chem.* **287**, 19355–19365 (2012).

Acknowledgments: We thank R. Guerreiro and J. Toombs. We thank B. Schmidt (Technical University of Darmstadt) for providing the inhibitor GI 254023X and P. Saftig (University Kiel) and Galderma for providing the inhibitor GL 506-3. We thank J. McCarter for critically reading the manuscript. We thank the personnel of the VIB Genetic Service Facility for the genetic screenings and the Antwerp Biobank at the Institute Born-Bunge for the autopsied brain and CSF samples. We also acknowledge the contribution of the clinical neurologists and the research nurses to the biosampling of the patients and the control individuals. **Funding:** This work was supported by the European Research Council under the European Union's Seventh Framework Program (FP7/2007-2013)/ERC Grant Agreement No. 321366-Amyloid (advanced grant to C.H.), the Deutsche Forschungsgemeinschaft (German Research Foundation) within the framework of the Munich Cluster for Systems Neurology (EXC 1010 SyNergy), the general legacy of Mrs. Ammer (to the Ludwig-Maximilians University/the chair of C.H.), and the Leonard Wolfson Institute for Experimental Neurology (to J.H.). This work was partly funded by the Instituto de Salud Carlos III (FISPI11/3035) to A.L. The Antwerp site was in part funded by the Belgian Science Policy Office Interuniversity Attraction Poles Program, the Flemish government–initiated Methusalem Excellence Program, the Alzheimer Research Foundation, the Medical Foundation Queen Elisabeth, the Research Foundation Flanders (FWO), the Agency for Innovation by Science and Technology Flanders (IWT), and the University of Antwerp Research Fund, Belgium. The IWT provides a PhD fellowship to E. Cuyvers, and the FWO provides a postdoctoral fellowship to J.v.d.Z. **Author contributions:** C.H. set up the research concept. G.K., M.S.-C., and C.H. designed the experiments and wrote the manuscript. G.K. and N.P. carried out all experiments except the TREM2 ELISA (fig. S3E), which was performed by Y.Y. under the supervision of M.C., and the phagocytosis assay with latex beads, which was carried out by E. Czirr under the supervision of T.W.-C. F.M. characterized cell lines and A.W.-W. and S.T. isolated and cultured primary microglia. J.H., M.C., M.S.-C., M.W., and S.L. provided valuable conceptual advice. M.S.-C. performed statistical analyses. E. Cuyvers, K.S., J.v.d.Z., and C.V.B. recruited patients, relatives, and control individuals; performed the genetic screening of AD and FTD genes; and provided mutation and clinical data of TREM2 mutation carriers. M.S.-C., E.L., H.S., A.L., D.A., J.F., J.L.M., J.-J.M., R.S.-V., A.A., A.R., M.T.H., A.D.-T., S.E., H.Z., and H.G. recruited patients and control persons and provided CSF samples. J.-J.M. performed autopsy diagnosis and provided neuropathology and immunohistochemistry data of AD and FTD patients. **Competing interests:** The authors declare that they have no competing interests.

Submitted 20 March 2014
Accepted 13 June 2014
Published 2 July 2014
10.1126/scitranslmed.3009093

Citation: G. Kleinberger, Y. Yamanishi, M. Suárez-Calvet, E. Czirr, E. Lohmann, E. Cuyvers, H. Struyfs, N. Pettkus, A. Wenninger-Weinzierl, F. Mazaheri, S. Tahirovic, A. Lleó, D. Alcolea, J. Fortea, M. Willem, S. Lammich, J. L. Molinuevo, R. Sánchez-Valle, A. Antonell, A. Ramirez, M. T. Heneka, K. Sleegers, J. van der Zee, J.-J. Martin, S. Engelborghs, A. Demirtas-Tatlidede, H. Zetterberg, C. Van Broeckhoven, H. Gurvit, T. Wyss-Coray, J. Hardy, M. Colonna, C. Haass, TREM2 mutations implicated in neurodegeneration impair cell surface transport and phagocytosis. *Sci. Transl. Med.* **6**, 243ra86 (2014).

www.sciencetranslationalmedicine.org/cgi/content/full/6/243/243ra86/DC1

Supplementary Materials for

TREM2 mutations implicated in neurodegeneration impair cell surface transport and phagocytosis

Gernot Kleinberger, Yoshinori Yamanishi, Marc Suárez-Calvet, Eva Czirr, Ebba Lohmann, Elise Cuyvers, Hanne Struyfs, Nadine Pettkus, Andrea Wenninger-Weinzierl, Fargol Mazaheri, Sabina Tahirovic, Alberto Lleó, Daniel Alcolea, Juan Fortea, Michael Willem, Sven Lammich, José L. Molinuevo, Raquel Sánchez-Valle, Anna Antonell, Alfredo Ramirez, Michael T. Heneka, Kristel Sleegers, Julie van der Zee, Jean-Jacques Martin, Sebastiaan Engelborghs, Asli Demirtas-Tatlidede, Henrik Zetterberg, Christine Van Broeckhoven, Hakan Gurvit, Tony Wyss-Coray, John Hardy, Marco Colonna, Christian Haass*

*Corresponding author. E-mail: christian.haass@dzne.lmu.de

Published 2 July 2014, *Sci. Transl. Med.* **6**, 243ra86 (2014)
DOI: 10.1126/scitranslmed.3009093

The PDF file includes:

Materials and Methods
Fig. S1. Absence of TREM2 fragments containing C-terminal FLAG tag.
Fig. S2. Analysis of maturation of TREM2.
Fig. S3. Characterization of BV2 cells stably overexpressing human TREM2.
Fig. S4. Characterization of novel sTREM2 ELISA.
Fig. S5. Impaired phagocytosis by mutant TREM2.
Table S1. Primers used for RT-PCR analysis.
Table S2. Characterization of novel sTREM2 ELISA.
Table S3. Spike recovery and linearity test for CSF and plasma sTREM2 ELISA.
References (*44–48*)

Science Translational Medicine
AAAS

Supplementary materials

Materials and Methods

cDNA constructs

The coding sequence of wild-type (WT) human TREM2 was amplified by PCR from a cDNA clone (Clone 693; Hölzel Diagnostika, Germany) introducing a HA-tag (YPYDVPDYA followed by the linker sequence SGGGGGLE) located after the endogenous TREM2 signal peptide (aa1-18) and a C-terminal FLAG tag (DYKDDDDK). TREM2 constructs were subcloned into the pcDNA5^{TM}/FRT/TO or into the pcDNA3.1/Zeo(+) vector (both Life Technologies) using the restriction enzymes HindIII (New England Biolabs) and XhoI (Thermo Scientific). The coding sequences of WT human DAP12, including a C-terminal V5-epitope tag (GKPIPNPLLGLDST), as well as the TREM2-DAP12 fusion constructs were generated using the Gibson Assembly^{TM} Method (New England BioLabs) using one or two gBlock Gene fragments (Integrated DNA Technologies), respectively, together with the pcDNA5^{TM}/FRT/TO vector linearized with the restriction enzymes BamHI and XhoI (Thermo Scientific). TREM2-DAP12 fusion constructs were designed according to Hamerman et al. (*25*), including an amino acid change in the transmembrane domain of DAP12 from aspartic acid to alanine (p.D50A). Additionally the TREM2-DAP12 fusion constructs included a HA-tag after the endogenous TREM2 signal peptide as described above. The TREM2 missense mutations p.T66M (ACG>ATG), p.Y38C (TAT>TGT), p.R47H (CGC>CAC), p.C36A (TGC>GCC) and p.C60A (TGC>GCC) were introduced into the respective plasmids by site-directed mutagenesis (Stratagene, La Jolla, CA) and all constructs verified by DNA sequencing.

RT-PCR analysis

Total RNA was isolated from BV2 cells using the RNeasy Mini Kit (Qiagen) and reverse transcribed into cDNA using the M-MLV reverse transcriptase Kit (Promega) according to the manufacturer's recommendations. Equal amounts of cDNA were amplified using Phusion® High-Fidelity DNA Polymerase (New England Biolabs) and PCR products separated on a 1% agarose gel. The primers used are listed in Table S1.

Mice

All animal experiments were performed in accordance with animal handling laws. Trem2 knockout ($Trem2^{-/-}$) mice (*24*) were maintained on a C57BL/6J background. Housing conditions included standard pellet food and water provided *ad libitum*, 12-hour light-dark cycle at temperature of 22 °C with cage replacement once per week and regular health monitoring. For isolation of primary microglia, postnatal day P5-P6 mice were scarified by decapitation.

siRNA and cDNA transfections and inhibitor treatments

For RNA interference, cells were reverse transfected with siGENOME pool targeting ADAM10 (10 nM; Thermo Scientific) or respective controls using Lipofectamine RNAiMAX transfection reagent (Life Technologies) according to the manufacturer's recommendations. Fresh medium was added 48 h post transfection and conditioned medium and lysates prepared 18-20h later as described below. Transient transfections of microglia BV2 cell cells were performed using Lipofectamine®2000 (Life Technologies) according to the manufacturer's recommendations. To study proteolytic processing of ectopically expressed WT human TREM2 or endogenously expressed murine Trem2, cells were treated with inhibitors essentially as described earlier (*44*). Inhibitors used were, GM 6001 (25 μM, Enzo Life Sciences), the ADAM10-specific inhibitor GI 254023X (5 μM, a kind gift from Dr. Schmidt, Technical University of Darmstadt, described previously (*45*)), the ADAM17-specific inhibitor GL 506-3 (5 μM, a kind gift from Galderma), the BACE1 inhibitor C3 (*46*) (5 μM). Cells were generally incubated for 18-20 h with respective inhibitors or vehicle controls before harvesting conditioned medium and preparation of membrane lysates.

Antibodies

For immunoblot detection, the following antibodies were used: goat polyclonal antibody against the N-terminus of human TREM2 (1:1,000 - 1:2,000; R&D Systems, AF1828), mouse monoclonal anti-FLAG M2 (1:4,000; Sigma), rat monoclonal anti-HA conjugated to HRP (3F10; 1:4,000; Roche), mouse monoclonal anti-V5 (1:5,000; Life Technologies), rabbit polyclonal anti-ADAM10 (1:4,000; Calbiochem), mouse monoclonal to

APP (22C11; 1:5,000; Millipore) and rabbit-anti calnexin (1:3000; Enzo Life Sciences). Secondary antibodies were HRP-conjugated goat anti-mouse, goat anti-rabbit IgG (1:10,000; both Promega), or anti-goat IgG (1:10,000; Santa Cruz Biotechnology). For immunocytochemistry rat monoclonal anti-HA (3F10; 1:100; Roche), rabbit polyclonal anti-calnexin (1:100; Enzo Life Sciences) and mouse monoclonal anti-giantin (1:100; Alexis) were used.

Immunofluorescence staining

HEK293 Flp-In cells stably overexpressing or BV2 cells transiently overexpressing TREM2 cDNA constructs were grown on poly-L-lysine-coated glass coverslips and fixed for 15 min in 4% paraformaldehyde (PFA) and 4% sucrose in phosphate-buffered saline (PBS). For intracellular staining cells were quenched with 50 mM NH_4Cl and permeabilized with 0.2% Triton X-100 in PBS for 5 min. For surface staining the permeabilization step was omitted. Fixed cells were blocked at room temperature (RT) with 5% normal goat serum in PBS for 30 min, subsequently incubated with indicated primary antibodies for 1 h at RT and visualized with corresponding secondary antibodies conjugated to Alexa Fluor-488 or Alexa Fluor-555 (Life Technologies). 4', 6-diamidino-2-phenylindol (Dapi, Life Technologies) was used as a nuclear counterstain. Images were acquired on a LSM700 confocal microscope using the Zen 2009 imaging software (Zeiss).

Surface biotinylation

Surface biotinylations were either carried out using HEK293 Flp-In cells stably overexpressing TREM2 cDNA constructs grown overnight on poly-L-lysine-coated dishes or with transiently transfected BV2 microglia cells which were analyzed 48 h post transfection. Cells were washed three times with cold PBS and incubated for 30 min at RT with PBS containing 0.5 mg/ml EZ-Link sulfo-NHS-LC Biotin (Pierce). Cells were washed three times with PBS and quenched with 50 mM NH_4Cl containing 1% bovine serum albumin (BSA) in PBS for 10 min at RT. After additional three washing steps in PBS, cells were harvested in PBS and lysed for 20 min on ice in cell lysis buffer (150 mM NaCl, 50 mM Tris-HCl, pH 7.6, 2 mM EDTA, 1% Triton-X 100) freshly supplemented with protease inhibitor cocktail (Sigma). Protein concentrations were measured using the bicinchoninic acid (BCA) method (Pierce) and equal amounts of protein were subject to precipitation using Streptavidin

sepharose (GE Healthcare) overnight at 4°C. Streptavidin sepharose was washed once with 1 ml of each STEN-NaCl (500 mM NaCl, 50 mM Tris-HCl, pH 7.6, 2 mM EDTA, 0.2% NP-40), STEN-SDS (150 mM NaCl, 50 mM Tris-HCl, pH 7.6, 2 mM EDTA, 0.2% NP-40, 0.1 (w/v) SDS), STEN (150 mM NaCl, 50 mM Tris-HCl, pH 7.6, 2 mM EDTA, 0.2% NP-40) and proteins eluted by boiling in 2x Laemmli sample buffer supplemented with beta mercaptoethanol for 10 min at 95°C. Note that no calnexin reactivity was detected on the immunoblots from streptavidin-precipitated samples confirming the integrity of the cells during the surface biotinylation procedure.

Metabolic labeling and immunoprecipitation

To analyze expression and maturation of TREM2, metabolic labeling experiments were performed similar to previously described methods (*47*). TREM2 was immunoprecipitated from medium and cell lysates using beads conjugated to a monoclonal anti-HA antibody (Sigma) and separated by standard 15% SDS-PAGE.

Preparation of conditioned media, cell lysates and immunoblotting

HEK293 Flp-In cells stably overexpressing TREM2 or TREM2-DAP12 cDNA constructs were seeded at a density of $1.5x10^5/cm^2$ and medium changed 48 h post seeding. Conditioned medium was collected after 18-20 h, immediately cooled down on ice, centrifuged at 13,000 rpm for 15 min at 4°C and supernatants frozen at -20°C until analysis. Transiently transfected BV2 cells were analysed either 24 h (inhibitor experiments) or 48 h post transfection. Supernatants were either immunoprecipitated with beads conjugated to a monoclonal anti-HA antibody (Sigma) or directly subjected to standard 15% SDS-PAGE. To prepare membrane fractions, cells were washed twice with ice-cold PBS, resuspended in ice-cold hypotonic buffer (0.01 M Tris, pH 7; 1 mM EDTA; 1 mM EGTA) freshly supplemented with protease inhibitor (Sigma) and incubated on ice for 30 min. After snap freezing in liquid nitrogen and thawing, the disrupted cells were centrifuged at 13,000 rpm for 45 min at 4°C. The resulting pellet was resuspended in STE lysis buffer (150 mM NaCl, 50 mM Tris-HCl, pH 7.6, 2 mM EDTA, 1% Triton-X 100), incubated for 20 min on ice and clarified by centrifugation at 13,000 rpm for 30 min at 4°C. Protein concentrations were measured using the BCA method, equal amounts of protein were mixed with Laemmli sample buffer supplemented with beta mercaptoethanol, separated by SDS-PAGE and transferred onto

polyvinylidene difluoride membranes (Hybond P; Amersham Biosciences, Aylesbury, UK). Bound antibodies were visualized by corresponding HRP-conjugated secondary antibodies using enhanced chemiluminescence technique (Pierce). Quantification of immunoblots was performed on a LAS-4000 image reader and analyzed using the Multi-Gauge V3.0 software (both Fujifilm Life Science).

Supplementary Figures

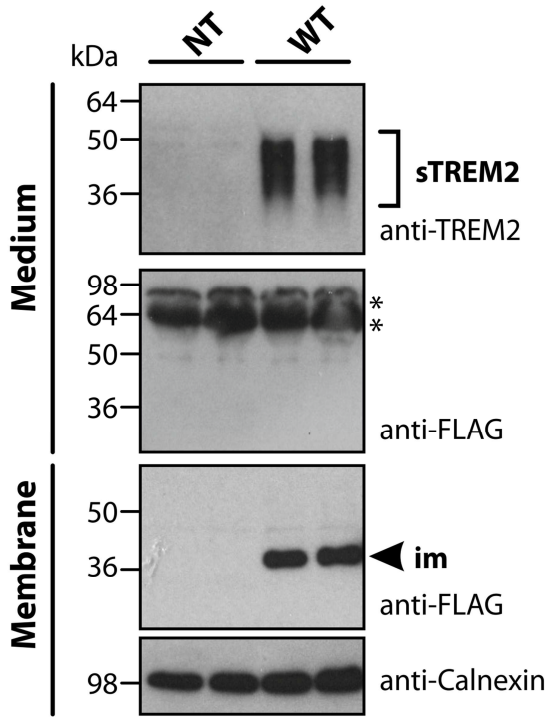

Fig. S1. Absence of TREM2 fragments containing C-terminal FLAG tag. Absence of specific TREM2 reactivity as shown by anti-FLAG immunoblotting of conditioned media confirms the generation of sTREM2 (upper panel) by ectodomain shedding. Anti-FLAG immunoblotting of the respective membrane fractions confirms the ability of the anti-FLAG antibody to detect the immature (im, black arrowhead) TREM2 protein. Anti-calnexin was used as loading control for the membrane fraction. NT, non-transfected HEK293 Flp-In host cell line; WT, TREM2 wild-type; im, immature; sTREM2, soluble TREM2. Asterisk indicates non-specific bands.

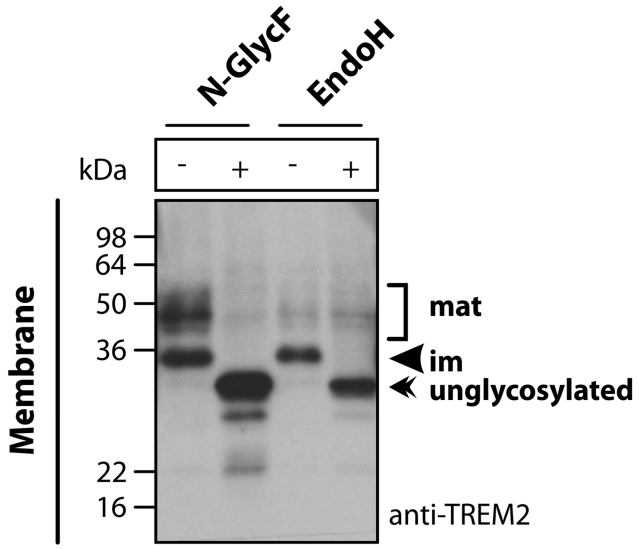

Fig. S2. Analysis of maturation of TREM2. Membrane fractions of HEK293 Flp-In cells stably expressing WT TREM2 were treated either with or without N-glycosidase F (N-GlycF) or Endoglycosidase H (EndoH) as previously described (*48*) and analysed by immunoblotting. Both treatment with N-GlycF and EndoH results in a shift of immature TREM2 while surface exposed TREM2 is complex glycosylated as shown by the partial resistance to EndoH and therefore is considered as fully mature TREM2.

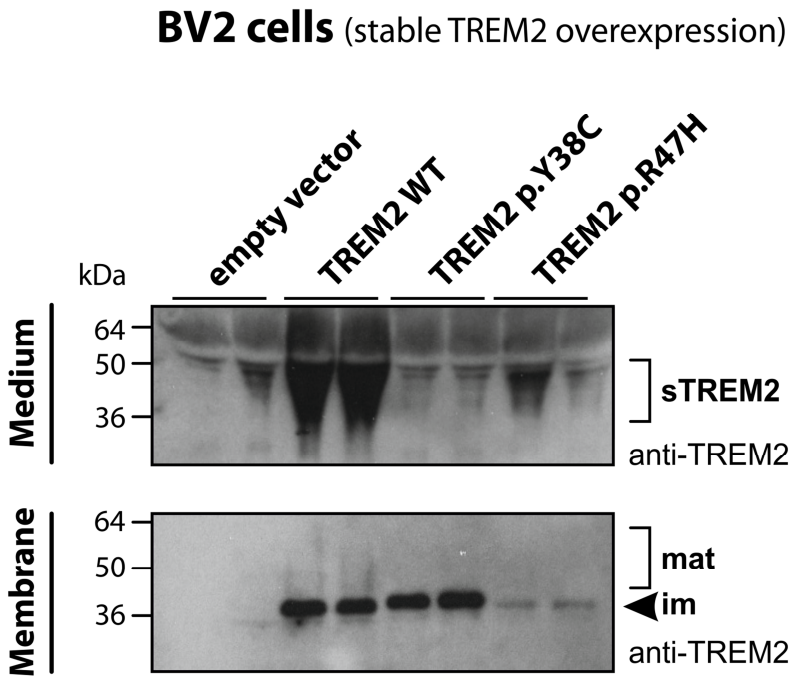

Fig. S3. Characterization of BV2 cells stably overexpressing human TREM2. Stable overexpression of wild-type (WT), TREM2 p.Y38C or TREM2 p.R47H mutant in the microglial BV2 cell line results in reduced generation of mutant sTREM2 (upper panel) accompanied with a slight increase of immature TREM2 p.Y38C in the membrane fraction (middle panel) and absence of mature TREM2. Note that the expression levels of the p.R47H variant upon stable overexpression was also lower compared to WT similar than upon transient transfection (Fig. 4B).

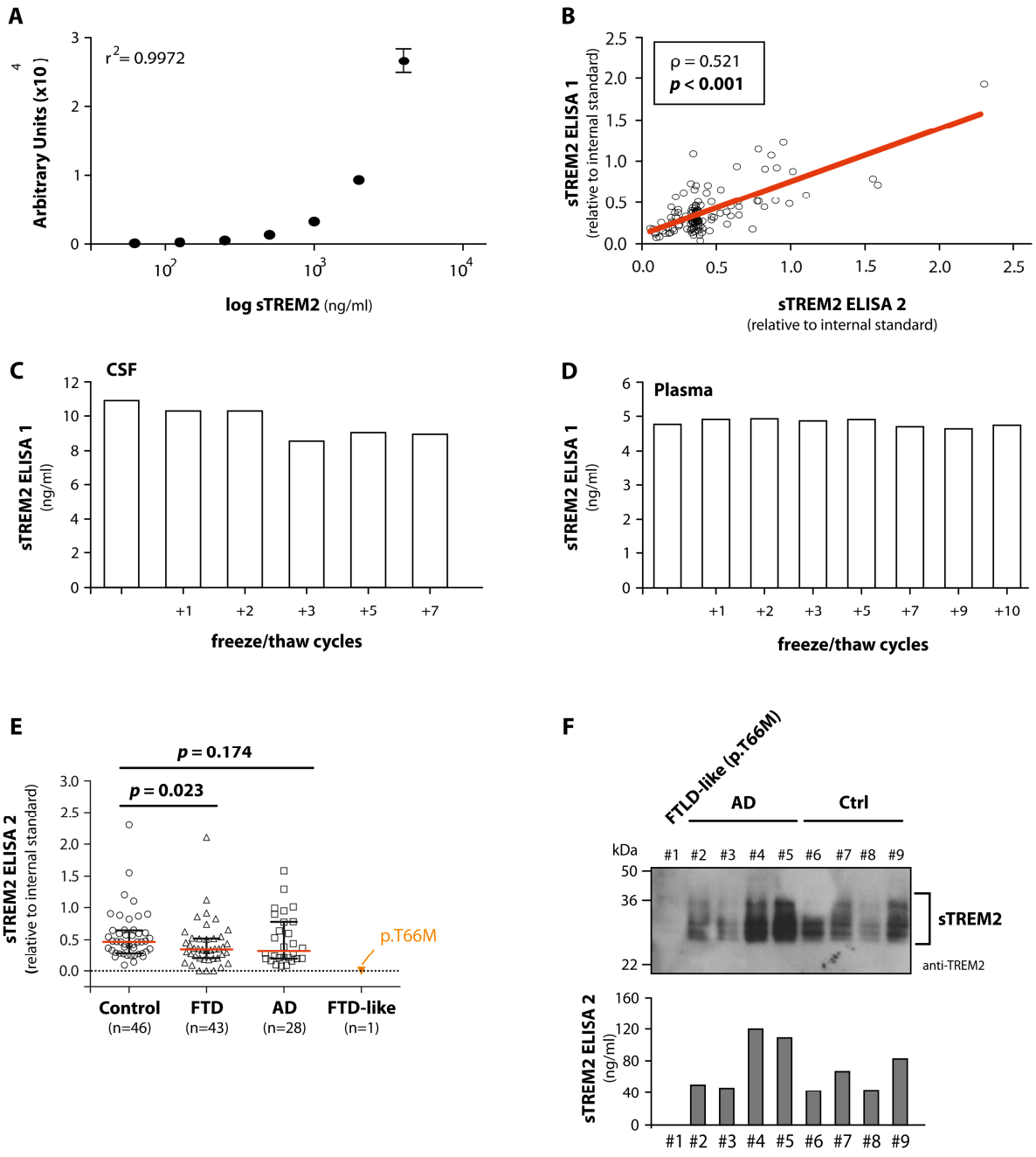

Fig. S4. Characterization of novel sTREM2 ELISA. (A) Standard curve of newly established sTREM2 ELISA using recombinant TREM2 ectodomain. **(B)** Correlation of the newly established sTREM2 ELISA with the previously published sTREM2 ELISA (*16*) shows a highly significant correlation between the two ELISAs. (Spearman rho = +0.521; $p<0.001$) **(C and D)** Analysis of repeated freeze/thaw cycles on sTREM2 levels in CSF **(C)** and plasma **(D)** shows that repeated freeze/thaw cycles have only a minimal effect on sTREM2 levels. **(E)** ELISA analysis of sTREM2 in CSF samples using a previously

published ELISA (*16*) confirms the absence of sTREM2 in the TREM2 p.T66M mutation carrier whereas robust levels of sTREM2 were detected in controls (n=46). Significantly reduced levels of sTREM2 were observed in FTD patients (n=43; $P_{\text{control vs. FTD}}$ = 0.023, Mann-Whitney U-Test). AD patients (n=28) also showed reduced sTREM2 levels compared to controls but this difference did not reach statistical significance ($P_{\text{control vs. AD}}$ = 0.174, Mann-Whitney U-Test). Horizontal bars indicate median sTREM2 levels per group with the interquartile range. **(F)** Selected CSF samples were analyzed for sTREM2 by immunoblotting using an independent TREM2 antibody. Comparing immunoblot intensities to individual ELISA readings revealed a high degree of correlation confirming the specificity of the TREM2 ELISA measurements.

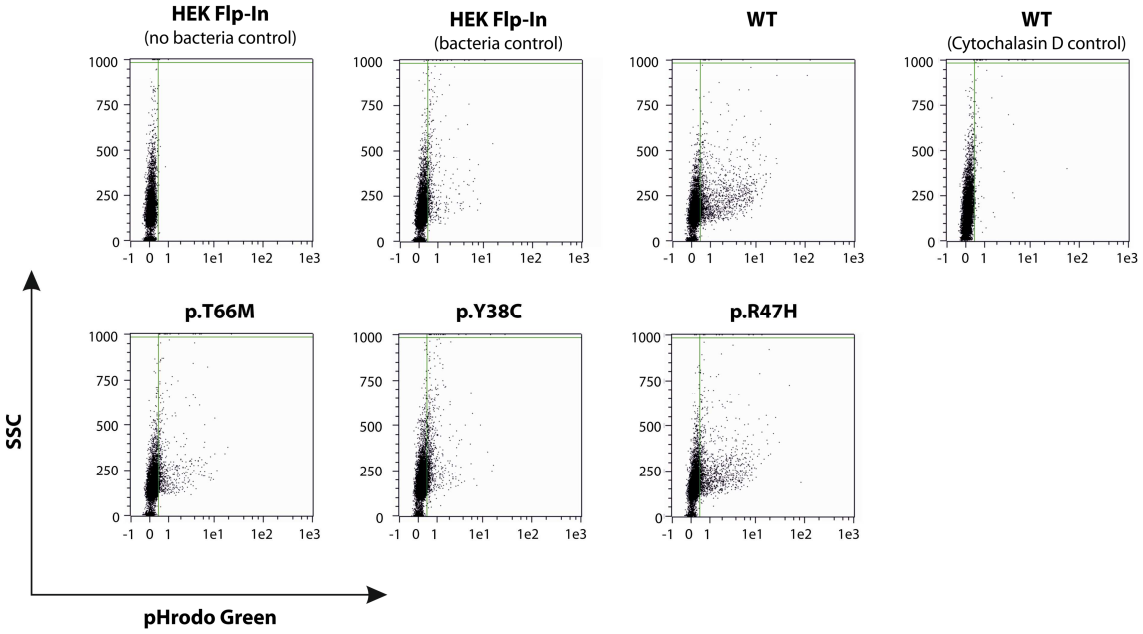

Fig. S5. Impaired phagocytosis by mutant TREM2. Phagocytosis of pHrodo *E.coli* in cells stably expressing TREM2-DAP12 fusion constructs and quantified by flow cytometry. Representative scatterblots for the quantification in Fig. 6G are shown for each condition.

Table S1. Primers used for RT-PCR analysis.

	Forward (5'-3')	**Reverse (5'-3')**
Dap12	CACCATGGGGGCTCTGGAGCCCTCCTGGTGCC	TCATCTGTAATATTGCCTCTGTGTGTTGAGG
Trem2	TGCCATGGGACCTCTCCACCAGTTTCTCCTGCTGC	TCAGAATTCTCTCACGTACCTCCGGGTCC
CD11b	CAGATCAACAATGTGACCGTATGGG	CATCATGTCCTTGTACTGCCGCTTG
CD68	GACCTACATCAGAGCCCGAG	AGAGGGGCTGGTAGGTTGAT
Gapdh	GGTGAAGGTCGGTGTGAACG	TTGGCTCCACCCTTCAAGTG

Table S2. Characterization of novel sTREM2 ELISA.

	Mean (±SD) [ng/ml]	**CV (%)**
Interplate variability		
Standard 1 (CSF)	*2.2 (±0.28)*	*13%*
Standard 2 (CSF)	*6.7 (±0.39)*	*6%*
Standard 3 (Plasma)	*2.7 (±0.14)*	*5%*
Standard 4 (Plasma)	*5.9 (±0.29)*	*5%*
Interday variability		
Standard 1 (CSF)	*2.2 (±0.28)*	*12%*
Standard 2 (CSF)	*6.7 (±0.14)*	*2%*
Standard 3 (Plasma)	*2.7 (±0.04)*	*1%*
Standard 4 (Plasma)	*5.9 (±0.09)*	*1%*

Abbreviations: CSF, cerebrospinal fluid; CV, coefficient of variance

Table S3. Spike recovery and linearity test for CSF and plasma sTREM2 ELISA.

	sTREM2 concentration [ng/ml]*		spike recovery (%)	Linearity (%)
	neat sample	spiked sample		
CSF	*4.8*	*10.2*	*108.3*	*95.7*
Plasma	*5.3*	*11.3*	*81.0*	*106.6*

Spike-recovery studies were performed using different concentrations of capture and detection antibody as well as different dilutions of the CSF and plasma samples in the assay diluent. The CSF and plasma samples were spiked with 5ng/ml of the recombinant sTREM2 standard and measured in the ELISA along with non-spiked samples. Spike recovery was calculated as the percent recovery of the signal above the signal levels in non-spiked samples. A concentration of 0.25 µg/ml of the capture antibody, 1 µg/ml of the detection antibody and a 1/4 dilution of the CSF and plasma samples showed the best recovery and linearity percentage (data shown in the table). *non-normalized data.